New Phytologist

Research

Dynamic monitoring of TGW6 by selective autophagy during grain development in rice

Zinan Liu[1]*, Qianying Yang[1]*, Pingfan Wu[1]*, Yifan Li[1]*, Yanni Lin[1]*, Wanqing Liu[1,2], Shaoying Guo[1], Yunfeng Liu[3], Yifeng Huang[4], Peng Xu[5], Yangwen Qian[6] and Qingjun Xie[1]

[1]State Key Laboratory for Conservation and Utilization of Subtropical Agro-Bioresources, Key Laboratory for Enhancing Resource Use Efficiency of Crops in South China, Ministry of Agriculture and Rural Affairs, Guangdong Provincial Key Laboratory of Plant Molecular Breeding, College of Agriculture, South China Agricultural University, Guangzhou, 510642, China; [2]Guangdong Academy of Agricultural Sciences, Rice Research Institute, Guangzhou, 510640, China; [3]State Key Laboratory for Conservation and Utilization of Subtropical Agro-Bioresources, College of Life Sciences and Technology, Guangxi University, Nanning, 530004, China; [4]Institute of Crop and Nuclear Technology Utilization, Zhejiang Academy of Agricultural Science, Hangzhou, 310001, China; [5]CAS Key Laboratory of Tropical Plant Resources and Sustainable Use, The Xishuangbanna Tropical Botanical Garden, Chinese Academy of Sciences, Menglun, Mengla, Yunnan, 666303, China; [6]WIMI Biotechnology Co. Ltd., Changzhou, 213000, China

Author for correspondence:
Qingjun Xie
Email: qjxie@scau.edu.cn

Received: *9 August 2023*
Accepted: *31 August 2023*

New Phytologist (2023)
doi: 10.1111/nph.19271

Key words: ATG, autophagy, grain quality, grain size, rice, TGW6.

Summary

- Crop yield must increase to achieve food security in the face of a growing population and environmental deterioration. Grain size is a prime breeding target for improving grain yield and quality in crop.
- Here, we report that autophagy emerges as an important regulatory pathway contributing to grain size and quality in rice. Mutations of rice *Autophagy-related 9b* (*OsATG9b*) or *OsATG13a* causes smaller grains and increase of chalkiness, whereas overexpression of either promotes grain size and quality.
- We also demonstrate that THOUSAND-GRAIN WEIGHT 6 (TGW6), a superior allele that regulates grain size and quality in the rice variety Kasalath, interacts with OsATG8 via the canonical Atg8-interacting motif (AIM), and then is recruited to the autophagosome for selective degradation. In consistent, alteration of either *OsATG9b* or *OsATG13a* expression results in reciprocal modulation of TGW6 abundance during grain growth. Genetic analyses confirmed that knockout of *TGW6* in either *osatg9b* or *osatg13a* mutants can partially rescue their grain size defects, indicating that TGW6 is one of the substrates for autophagy to regulate grain development.
- We therefore propose a potential framework for autophagy in contributing to grain size and quality in crops.

Introduction

Population growth, climate change, and decreases in arable land area create demand for higher crop yields (Butardo *et al.*, 2019; Park *et al.*, 2019). Breeding new elite rice varieties with high-yield and superior-quality is definitely desired (Ren *et al.*, 2023). Grain size is a key determinant for both yield and quality and thus a prime target for cereal crop breeding. However, rice yield and quality are usually antagonistic to each other due to the complex trade-off between agronomic traits underlying grain size and grain quality, thereby preventing the application of the cloned grain-associated genes deployed in rice breeding (Ren *et al.*, 2023). For example, increase in grain size by photosynthetic carbon fixation driving carbohydrates translocation from vegetative source organs generally results in the decrease in eating and cooking quality (ECQ) in grain, which stems from the accumulation of carbohydrates and its derivatives in the endosperm, such as storage starch (Butardo *et al.*, 2019). Therefore, further elucidating the crosstalk between the known regulatory pathways governing grain size and quality, and deciphering potential novel gene resources have become one of the most important issues to be tackled.

Autophagy is a highly conserved 'self-eating' mechanism executing the degradation of unneeded components in bulk for nutrient recycling and metabolic homeostasis, eventually facilitating the survival of plants under suboptimal environments (Marshall & Vierstra, 2018). To date, the regulatory mechanism of autophagy and the scores of the responsible components have been well-documented, especially Autophagy-related (ATG) proteins. The ATGs and other components together operate the canonical route of autophagic machinery. Briefly, ATG13 is rapidly dephosphorylated, which then leads to enhancing ATG1–ATG13 interaction, as well as ATG13–ATG17 binding, resulting in the formation of the ATG1 kinase complex. Once

*These authors contributed equally to this work.

activated, the ATG1 kinase complex would then recruit other downstream ATG proteins to initiate autophagosome formation (Li *et al.*, 2014; Yao *et al.*, 2023). ATG9 is a lipid scramblase that is activated and incorporated into a vesicle (termed ATG9 vesicle) at the Golgi apparatus, and then is recruited to the phagophore assembly site (PAS) and functions as an initial membrane source for the isolation membrane (IM; Zhuang *et al.*, 2017; Matoba *et al.*, 2020). Subsequently, the decoration of the phagophore is performed by the conjugation of ATG8 to phosphatidylethanolamine (PE; termed as ATG8-PE) adduct (Marshall & Vierstra, 2018). Meanwhile, ATG8 interacts with cargo receptors or proteins containing either the Atg8-interacting motif (AIM) that is consist of consensus sequences (W/F/Y–X–X–V/I/L) or the newly defined ubiquitin-interacting motif (UIM), and then delivers them into the autophagosome for degradation within the vacuole (Noda *et al.*, 2010; Farré *et al.*, 2017; Marshall *et al.*, 2019).

Autophagy in plant is mainly evident to function in response to various stresses (Marshall & Vierstra, 2018). Relatively, roles of autophagy in terms of plant growth and development still remain extensively elusive. To date, several biological functions of *ATGs* have been characterized, including regulating pollen development, leaf senescence, and seedling growth, nitrogen use efficiency (NUE) in plants, as well as grain yield (Kurusu *et al.*, 2014; Li *et al.*, 2015; Wada *et al.*, 2015; Erlichman *et al.*, 2023). For example, overexpressing *OsATG8a* significantly increases the grain yield, grain number, and panicle number (Yu *et al.*, 2019; Fan *et al.*, 2020). A recent study reveals a new mechanism underlying Heading date 1 (Hd1) protein homeostasis by which Hd1 is degraded by autophagy for controlling rice flowering (Hu *et al.*, 2022). Moreover, the selective autophagy cargo receptor OsNBR1 was reported to deliver the Brown Planthopper 14 (BPH14)-interacting salivary protein (BISP) to OsATG8 for degradation, thereby enabling rice to resist the BPHs without compromising yield performance in the natural habitats (Guo *et al.*, 2023). However, it is still an open issue that if autophagy can be exploited to boost agronomic productivity and yield by altering the degradation of specific constituents (Marshall & Vierstra, 2018), in particular the traits directly related to yield and quality, such as grain size and quality in cereal crops.

THOUSAND-GRAIN WEIGHT 6 emerged during breeding selection of rice (*Oryza sativa*; Ishimaru *et al.*, 2013) as a superior target and has been successfully deployed for molecular breeding of high-yielding elite varieties with superior grain quality (Li *et al.*, 2019; Mao *et al.*, 2021). Loss of function of *TGW6* increases the grain length and grain yield, accompanied with the lower chalky grain ratio under high temperature (Ishimaru *et al.*, 2013). Notably, how TGW6 is dynamically regulated during grain development is still unclear, which limits its further exploitation.

Here, we demonstrate that autophagic machinery controls TGW6-mediated grain development in rice. Therefore, our findings uncover a novel regulation mechanism of the TGW6, and manipulation of ATGs-TGW6 module likely enables the potential for simultaneously improving grain size and quality in crops.

Materials and Methods

Plant materials and growth conditions

Oryza sativa subsp. *japonica* cv Zhonghua 11 (ZH11, WT) was used in this study. The knockout mutants *osatg9b*, *osatg13a*, *osatg5*, *osatg7*, and *tgw6* were generated by CRISPR/Cas9-mediated gene editing (Supporting Information Fig. S1). To generate the double-knockout mutants of *tgw6 osatg9b*, *tgw6 osatg13a-1*, *tgw6 osatg13a-2*, and *tgw6 osatg13a-3*, *TGW6* was mutated by CRISPR/Cas9-mediated gene editing in the *osatg9b* or *osatg13a-1* background, respectively (Fig. S1c). The detailed editing sequences were shown in Table S1. T1 generation lines of each allelic mutation were back-crossed once, and then the resulting homozygous allelic lines without transgenes were identified and selected for the study. In transgenic plants overexpressing *OsATG9b*, *OsATG13a*, or *OsATG8b*, the transgenes were driven by the maize *Ubiquitin* promoter. All transgenes and corresponding binary plasmids were sequencing-verified and then transformed into Agrobacterium (*Agrobacterium tumefaciens*) strain EHA105 before being transformed into ZH11 or corresponding *osatgs* mutants calli. More than 20 independent positive calli (T0) were obtained, and five independent T2 homozygous overexpression lines for *OsATG9b*, *OsATG13a*, and *OsATG8b* each were chosen for this study. Line no. 1 of *OE-OsATG9b* was selected as a representative for this study because it had the highest expression level of *OsATG9b* (Fig. S2), as well as line no. 1 of *OE-OsATG13a* (Fig. S3). To generate the *osatg9b-C* complementation line, the *Ubi*::*pro*:*OsATG9b-GFP* construct was transformed into the *osatg9b* mutant. To generate *osatg9b OE-OsATG8b* and *osatg13a OE-OsATG8b* transgenic plants, *Ubipro*::*GFP-OsATG8b* transgenic plants were crossed with *osatg9b* and *osatg13a*, respectively, and the homozygous *osatg9b OE-OsATG8b* and *osatg13a OE-OsATG8b* were selected for this study.

Plants were grown and routinely managed at the paddy field in the South China Agricultural University Wushan Campus Teaching & Research Base (Guangzhou, China, 113°21′E, 23°9′N), Zengcheng Campus Teaching & Research Base (Guangzhou, China, 113°49′E, 23°18′N), and Lingshui (Hainan, China, 18°22′E, 109°45′N). *Nicotiana benthamiana* seedlings were grown in a growth chamber at 28°C under a 16 h : 8 h, light : dark photoperiod. Rice seeds were surface-sterilized using 70% (v/v) ethanol and 25% (v/v) NaClO and washed several times. Rice etiolated seedlings used for protoplasts isolation were grown on ½-strength Murashige and Skoog (½MS) medium with 3% (w/v) sucrose, and 0.8% (w/v) agar in the dark at 30°C for 1 wk.

Plasmid construction

To generate the overexpression lines of the *Ubipro*::*GFP-OsATG8b*, *Ubipro*::*RFP-OsATG8b*, *Ubipro*:*OsATG9b-GFP*, and *Ubipro*:*OsATG13a-GFP* constructs, the full-length coding sequences (CDSs) of them were individually amplified from ZH11 seedlings and then cloned into the binary vector

pCAMBIA1301. To knockout *OsATG9b*, *OsATG13a*, and *TGW6*, specific oligonucleotides for targeted mutagenesis were designed online (http://skl.scau.edu.cn/; Table S1) and then cloned into a CRISPR/Cas9 plant expression vector as described previously (Zeng *et al.*, 2018). The coding regions of *OsATG9b* (*Os10g0163100*), *OsATG13a* (*Os02g0644500*), *OsATG8a* (*Os07g0512200*), *OsATG8b* (*Os04g0624000*), *OsATG8c* (*Os08g0191600*), *OsATG8d* (*Os11g0100100*), and *TGW6* (*Os06g0623700*) were cloned to generate *pNC-Green-subN-OsATG8b* and *pNC-mCherry-N-TGW6* for subcellular localization analyses; *pMetYCgate-TGW6* and *pPR3-NubG-OsATG8s* (*OsATG8a-d*) for yeast-two hybrid (Y2H) assays; *TGW6-nEYFP* and *cEYFP-OsATG8s* for bimolecular fluorescence complementation (BiFC) assays; *TGW6-nLuc*, *cLuc-OsATG8s* for split luciferase complementation (LUC) assays; *TGW6-MBP* and *GST-OsATG8s* for pull-down assays. To generate the depletion of AIM2 or AIM3 in TGW6, we mutated the corresponding residues of the two AIMs to Alanine within full-length TGW6, resulting in TGW6$^{\triangle AIM2}$ (Y148A L150A) or TGW6$^{\triangle AIM3}$ (W282A L284A), respectively. To generate the deletions of LDS (LIR/AIM docking site) or UDS (UIM docking site) in OsATG8a, we mutated the corresponding residues of them into Alanine according to previous study (Marshall *et al.*, 2019), resulting in OsATG8a$^{\triangle LDS}$ (Y50A L51A) or OsATG8a$^{\triangle UDS}$ (I77A V78A V79A; Table S2). Then, the resulting *TGW6*$^{\triangle AIM2}$, *TGW6*$^{\triangle AIM3}$, *OsATG8a*$^{\triangle LDS}$, and *OsATG8a*$^{\triangle UDS}$ were individually cloned into *pNC-mCherry-N-TGW6*$^{\triangle AIM2}$, *pNC-mCherry-N-TGW6*$^{\triangle AIM3}$, *pMetYCgate-TGW6*$^{\triangle AIM2}$, *pMetYCgate-TGW6*$^{\triangle AIM3}$, *TGW6*$^{\triangle AIM2}$*-nEYFP*, *TGW6*$^{\triangle AIM3}$*-nEYFP*, *cEYFP-OsATG8a*$^{\triangle LDS}$, *cEYFP-OsATG8a*$^{\triangle UDS}$, *TGW6*$^{\triangle AIM2}$*-nLuc*, *TGW6*$^{\triangle AIM3}$*-nLuc*, *TGW6*$^{\triangle AIM2}$*-MBP*, and *TGW6*$^{\triangle AIM3}$*-MBP* for subcellular colocalization assays, Y2H assays, BiFC assays, LUC assays, and pull-down assays, respectively. All primers used for cloning are listed in Table S2. The constructs *mCherry-AtRER1B* (Golgi marker; Sato *et al.*, 1999; Takeuchi *et al.*, 2000), *mCherry-OsRac3* (PM marker; Chen *et al.*, 2010), *mCherry-KTI1* (ER marker; Jofuku & Goldberg, 1989), and *AtTZF1-mCherry* (cytosolic foci marker; M. C. Pomeranz *et al.*, 2010) were kindly provided by Prof. Yaoguang Liu (Han *et al.*, 2022).

Grain size measurement

Grain size traits described in this study (grain length and grain width) were measured using a rice digital seed test machine (Grainpheno). Grain size and the thousand-grain weight were measured in > 20 replicates, with each replicate consisting of > 500 grains.

Observations of spikelet hull cells

To observe the inner parenchyma cells of spikelet hulls, transverse sections of spikelet hulls were used to prepare semithin sections. Samples were stained with 1% (w/v) toluidine blue for 5 s and subsequently examined under an optical microscope (Motic BA200; Motic, Amoy, China).

The outer epidermal cells of spikelet hulls were observed in mature grains. The samples were observed under a ZEISS EVO MA 15 scanning electron microscope. The cell length, cell width, and lemma length were determined by ImageJ.

Protoplast isolation and transformation

The shoots of 1-wk-old rice seedlings were used for protoplast isolation with an enzymatic digestion solution (1.5% (w/v) cellulose R-10, 0.75% (w/v) macerozyme R-10, 0.4 M mannitol, 20 mM MES pH 5.7, 10 mM $CaCl_2$, 0.1% (w/v) BSA). The protoplasts were filtered through 100 µm nylon mesh and then washed with W5 solution (154 mM NaCl, 125 mM $CaCl_2$, 5 mM KCl, 2 mM MES pH 5.7) and suspended in MMG solution (0.4 M mannitol, 15 mM $MgCl_2$, 4 mM MES pH 5.7). An equal volume of 40% PEG solution (40% (w/v) PEG 4000, 0.1 M $CaCl_2$, 0.2 M mannitol) was added to the prepared protoplast cells that contained plasmid DNAs. Finally, the transformed protoplasts were washed with W5 solution and incubated in W5 solution overnight in the dark.

Subcellular localization

Protoplasts were isolated from 10-d-old rice seedlings. For subcellular colocalization of *OsATG13a*, the *Ubipro:OsATG13a-GFP* was cotransfected with the different organelles marker, respectively, including *mCherry-AtRER1B* (Golgi marker), *mCherry-OsRac3* (PM marker), *mCherry-KTI1* (ER marker), *AtTZF1-mCherry* (cytosolic foci marker), as well as with *Ubipro::RFP-OsATG8b*; for subcellular colocalization of *OsATG9b*, the *Ubipro:-OsATG9b-GFP* was cotransfected with *mCherry-AtRER1B* (Golgi marker) or *Ubipro::RFP-OsATG8b* as reported previously (Zhang *et al.*, 2011). To determine the localization pattern of TGW6 with OsATG8b, the *pNC-Green-subN-OsATG8b* and *pNC-mCherry-N-TGW6* were transformed into Agrobacterium GV3101 pSoup, and subsequently cotransformed into the leaves of *N. benthamiana* as reported (Sparkes *et al.*, 2006). The fluorescence signal was observed using a laser scan confocal microscope (Leica STELLARIS 5; Leica, Wetzlar, Germany).

Autophagy induction or inhibition treatment

The root tips of 7-d-old WT, *osatg9b*, *osatg13a*, *OE-OsATG9b*, and *OE-OsATG13a* seedlings were soaked in liquid ½MS medium containing 1 µM Concanamycin A (ConA; BVT-0237-M001; Adipogen, San Diego, CA, USA) or 1 µM wortmannin (52405ES03; Yeasen Biotechnology, Shanghai, China) for 12 h in the dark as reported (Izumi *et al.*, 2015). Monodansylcadaverine (MDC; 30432; Sigma-Aldrich) staining was performed according to previous report (Pu & Bassham, 2016). In terms of transient investigation of autophagy activity, rice protoplasts were cultured in W5 solution containing 1 µM ConA for 12 h in the dark according to previous report (Nolan *et al.*, 2017).

In *N. benthamiana*, transient expression was performed by leaf agroinfiltration as reported previously (Luo *et al.*, 2023). For ConA treatment, leaves were infiltrated with 1 µM ConA solution for 36 h after Agrobacterium infiltration as reported (Luo *et al.*, 2023).

Testing of the anti-OsATG8 antibody and generation of the polyclonal anti-TGW6 antibody

The ATG8 antibody was purchased from Agrisera (AS14 2811; Agrisera, Vännäs, Sweden). To test the specificity of the anti-ATG8 antibody in rice, an immunoblot was performed on 10-d-old WT and *GFP-OsATG8b* seedlings. A band of *c.* 15 kDa representing OsATG8b was detected in both WT and *GFP-OsATG8b*; another specific band of *c.* 40 kDa representing the GFP-OsATG8b fusion was detected in the *GFP-OsATG8b* seedlings but not in WT (Fig. S4a). The same *c.* 40 kDa band was detected with an anti-GFP antibody; the anti-GFP antibody also detected a protein of *c.* 25 kDa representing free GFP in the *GFP-OsATG8b* seedlings (Fig. S4a), indicating that the anti-ATG8 antibody can be used to identify OsATG8b. The anti-TGW6 polyclonal antibody was produced by PhytoAB Company (San Jose, CA, USA) by using the specific peptide HHKVTGRRDR. The predicted molecular weight of full-length TGW6 is *c.* 38 kDa (Ishimaru *et al.*, 2013). A specific band of the appropriate size was detected by the anti-TGW6 antibody in WT but was absent in the *tgw6* mutant (Fig. S4b), indicating that the anti-TGW6 antibody specifically detects TGW6.

Protein isolation and immunoblot analysis

Total protein extraction was conducted using 2× SDS gel loading buffer (100 mM Tris–HCl pH 6.8, 4% (w/v) SDS, 0.2% (w/v) bromophenol blue, 20% (v/v) glycerol, 200 mmol l^{-1} DDT). OsATG8-PE detection was conducted according to the previous report (Chung *et al.*, 2010). Briefly, total protein was separated by SDS-PAGE with 6 M urea and blotted with a polyclonal antibody raised against *Arabidopsis* ATG8 to detect OsATG8 and OsATG8-PE. The GFP-OsATG8b detection was assessed as previous study (Izumi *et al.*, 2015). The calculation of GFP : GFP-OsATG8b ratio was determined by the intensity of free GFP moiety bands, normalized by the corresponding intensity of full-length GFP-OsATG8b bands. The anti-GFP antibody (632381; TaKaRa Bio, Kusatsu, Japan) was used in this study.

Quantification of the protein band intensity from immunoblots was performed with the software ImageJ. Each experiment was performed at least three times, and one representative result is shown.

Yeast split-ubiquitin system

Yeast-two hybrid assays were performed according to previous report (Song *et al.*, 2021). Cub and NubG were used as negative controls. The combinations of *pPR3-NubG-OsATG8s* (representing *cEYFP-OsATG8a*, *cEYFP-OsATG8b*, *cEYFP-OsATG8c*, and *cEYFP-OsATG8d*) with *pMetYCgate-TGW6*, *pPR3-NubG-OsATG8b* with *pMetYCgate-TGW6*$^{\triangle AIM2}$ and *pPR3-NubG-OsATG8b* with *pMetYCgate-TGW6*$^{\triangle AIM3}$) were co-infiltrated into strain NMY51 and examined on SD/−Trp/−Leu, SD/−Trp/−Leu/−His/−Ade and SD/−Trp/−Leu/−His/−Ade/X-Gal plates for 24–36 h. The interactions were verified by testing for LacZ activity.

BiFC assays

Bimolecular fluorescence complementation assays were performed according to previous report (Han *et al.*, 2022). The combinations of *TGW6-nEYFP* with *cEYFP-OsATG8s* (representing *cEYFP-OsATG8a*, *cEYFP-OsATG8b*, *cEYFP-OsATG8c*, and *cEYFP-OsATG8d*), *TGW6*$^{\triangle AIM2}$*-nEYFP* or *TGW6*$^{\triangle AIM3}$*-nEYFP* with *cEYFP-OsATG8b*, and *TGW6-nEYFP* with *OsATG8a*$^{\triangle LDS}$ or *OsATG8a*$^{\triangle UDS}$ were co-infiltrated into *N. benthamiana* leaves as previously reported (Sparkes *et al.*, 2006). YFP fluorescence was monitored using a confocal microscope (Leica STELLARIS 5).

LUC reporter assays

The combinations of *cLuc-OsATG8s* (representing *cLuc-OsATG8a*, *cLuc-OsATG8b*, *cLuc-OsATG8c*, and *cLuc-OsATG8d*) with *nLuc-TGW6*, *cLuc-OsATG8b* with *nLuc-TGW6*$^{\triangle AIM2}$ and *cLuc-OsATG8b* with *nLuc-TGW6*$^{\triangle AIM3}$) were transformed into Agrobacterium GV3101 pSoup, and the appropriate pairs of cell suspensions were infiltrated into *N. benthamiana* leaves as previously reported (Sparkes *et al.*, 2006). Subsequently, luciferase activity was measured using a dual-luciferase reporter assay system (E1910; Promega).

Pull-down assays

The recombinant proteins (GST-OsATG8s, TGW6$^{\triangle AIM2}$-MBP, TGW6$^{\triangle AIM3}$-MBP, TGW6-MBP, GST, and MBP) were purified from *Escherichia coli* strain BL21 and used for GST pull-down assays as reported previously (He *et al.*, 2023). Detection of GST- and MBP-fused proteins was performed with anti-GST (CW0084M; 1 : 5000; CWBIO, Beijing, China) and anti-MBP antibodies (E8032S; 1 : 5000; New England Biolabs, Ipswich, MA, USA), respectively.

Determination of AC and chalkiness

The percentage chalkiness is the number of grains showing chalkiness (as determined by visual assessment) divided by 100, sampled from random dehulled grains from each plant. The chalkiness degree was analyzed with a rice appearance quality detector (Greenpheno). The grain chalkiness ratio is the percentage of chalkiness multiplied by chalkiness degree. Flour ground from milled grain was used to measure the amylose starch content as previously described (Wu *et al.*, 2022).

RT-qPCR analysis

Total RNA was extracted from the indicated samples with Trizol reagent (P118-05; GenStar, Beijing, China) and first-strand cDNAs were synthesized using an Evo M-MLV Reverse Transcription Premix Kit (G490; Applied Biological Materials Inc., Richmond, BC, Canada). qPCR was performed with three biological replicates. Data are presented as means ± standard deviation (SD). The relative expression level of the tested genes was normalized to that of *OsUBIQUITIN1* (*OsUBI1*, LOC_Os06g46770) and

calculated by the $2^{-\Delta\Delta CT}$ method (Livak & Schmittgen, 2001). The primers used for qPCR are listed in Table S3.

Results

Involvements of *OsATG9b* and *OsATG13a* in regulation of grain size

The rice genome encodes 33 OsATGs, each participating in some aspects of autophagy (Xia *et al.*, 2011). Transcriptome profiling showed that 14 *OsATGs* are highly expressed in panicle (Fig. S5; Yang *et al.*, 2022), which might be the key factor directly related to yield and quality in rice. Among them, *OsATG5* and *OsATG7* are known to regulate heading date and pollen development that ahead of grain development (Kurusu *et al.*, 2014; Hu *et al.*, 2022) and thus was not adaptable for studying grain related traits in this study. Out of the rest *OsATGs*, we selected *OsATG13a*, encoding a putative autophagy induction component, and *OsATG9b*, encoding a putative autophagosome biogenesis component, as representatives to dissect the role of autophagy in regulating agronomic traits in rice since they are supposed to function in the key steps of autophagic machinery (induction of autophagy and formation of autophagosome, respectively; Marshall & Vierstra, 2018). ATG13 is a scaffold protein in ATG1 kinase complex, and its phosphorylation status-regulated phase separation controls the initiation of autophagy (Fujioka *et al.*, 2020; Qi *et al.*, 2022; Nguyen & Faesen, 2023). ATG9 is a scramblase that regulates phagophore expansion (Chumpen Ramirez *et al.*, 2023; Olivas *et al.*, 2023). We validated the high expression of *OsATG9b* in panicles at the heading stage and high expression of *OsATG13a* in the panicle 1 d after fertilization by reverse transcription quantitative PCR (RT-qPCR; Fig. 1a). Therefore, we speculated that these two *OsATGs* may be involved in regulating grain development.

To address above issue, we generated *osatg9b* and *osatg13a* mutants by clustered regularly interspaced short palindromic repeat (CRISPR)/CRISPR-associated nuclease 9 (Cas9)-mediated gene editing; we obtained one *osatg9b* allele with a 1-bp insertion, leading to a frameshift and the introduction of a premature stop codon (Fig. S1a). Phenotypic characterization revealed that the grain length of *osatg9b* was significantly reduced 10.9% as compared to that of wild-type (WT; Fig. 1b,d), but the grain width between *osatg9b* and WT was not significantly different (Fig. 1c,e), finally leading to the 18.5% loss of grain weight of *osatg9b* (Fig. 1f). In addition, the plant height, panicle length, and branch number of *osatg9b* were significantly reduced but the tiller number was significantly increased compared with those of WT (Fig. S6). Given only one allele of *osatg9b* was generated, a genetic complementation was performed to exclude the off-target editing effect for *osatg9* phenotype, showing that the grain defects of *osatg9b* mutant were fully rescued by the *OsATG9b* transgene (Fig. S7). Similarly, *osatg9b-C* exhibited normal plant height, panicle length, branch number, and tiller number, similar to that of WT (Fig. S6).

In respect to the *osatg13a* mutants, we generated two *osatg13a* alleles: *osatg13a-1* with a 13-bp deletion and *osatg13a-2* with a 4-bp deletion, both introducing premature stop codons (Fig. S1a). Similar to *osatg9b*, the average grain length of *osatg13a-1* and *osatg13a-2* were also reduced 13.2% and 11.5% as compared to that of WT (Fig. 1b,d), respectively. Interestingly, the average grain width of them was increased 14.0% and 13.7% as compared to that of WT (Fig. 1c,e), respectively, eventually leading to 20.6% and 13.6% decrease of thousand-grain weight (Fig. 1f), indicating that *OsATG13a* is responsible for both grain elongation and expansion. In addition, the plant height, panicle length, and tiller number of *osatg13a* were significantly reduced but branch number was significantly increased (Fig. S8).

To preclude the compensatory roles of *OsATG9a* and *OsATG13b* in *osatg9b* and *osatg13a* mutants, we examined the expression levels of *OsATG9a* and *OsATG13b* in their respective mutant lines. The results showed that the expression levels of *OsATG9a* and *OsATG13b* in their respective mutants were not significantly different from those in WT (Fig. S9), which indicated that the altered grains size were owned to the mutant themselves. Taken together, our results suggested that *OsATG9b and OsATG13a* are involved in grain growth in rice.

Alteration of the cell size in *osatgs* mutants

Spikelet hull is thought to dictate final grain size (Li *et al.*, 2019). To unravel the reason of grain defect in both *osatg9b* and *osatg13a*, cytological analyses of their spikelet hulls were executed and then demonstrated that the epidermal cell length and width of *osatg9b* were smaller than that of WT (Fig. 2a,b), while cell number of *osatg9b* was not significantly different from WT in the longitudinal but increased in the transverse directions (Fig. 2a,b). We observed similar changes in cell size and number in *osatg13a-1* (selected as the *osatg13a* mutant representative for the following studies), with a more pronounced increase in cell number in the transverse direction (Fig. 2a,b). We examined cross-sections of transverse sections from spikelet hulls at their apical region and observed that the palea in inner parenchymal cells (ipc) were significantly shorter in the *osatg9b* and *osatg13a-1* mutants compared with WT (Fig. 2c,d). These observations suggest that ipc length determines the final size of the cells.

To assess how *OsATG9b* and *OsATG13a* regulate grain development, we also investigated grain growth of *osatg9b* and *osatg13a-1* along nine developmental stages of spikelet from 3–5 to 23–25 cm in length. We observed that the grain length of both *osatg9b* and *osatg13a* mutants was different from that of WT from the 10 to 13 cm stage onward (Fig. 2e). Grain width in *osatg9b* was first reduced at the 8–10 cm stage compared with WT, but then returned to WT levels at the 15–17 cm stage (Fig. 2e), finally resulting in the same grain width in *osatg9b* and WT. Grain width of *osatg13a* gradually expanded from the 10 to 13 cm stage until maturity (Fig. 2e), eventually leading to the observed greater grain width phenotype in this mutant. Further analysis demonstrated that the shape of the *osatg13a* endosperm was distinctly abnormal from that of WT and *osatg9b* from days after fertilization (DAF) 5 (Fig. S10), seeming that the elongation of endosperm was limited by the hull. We thus proposed that this may be the cause of the greater width of *osatg13a*. Consistently, the expression of cell cycle genes was significantly upregulated in both *osatgs* mutants at the 3–

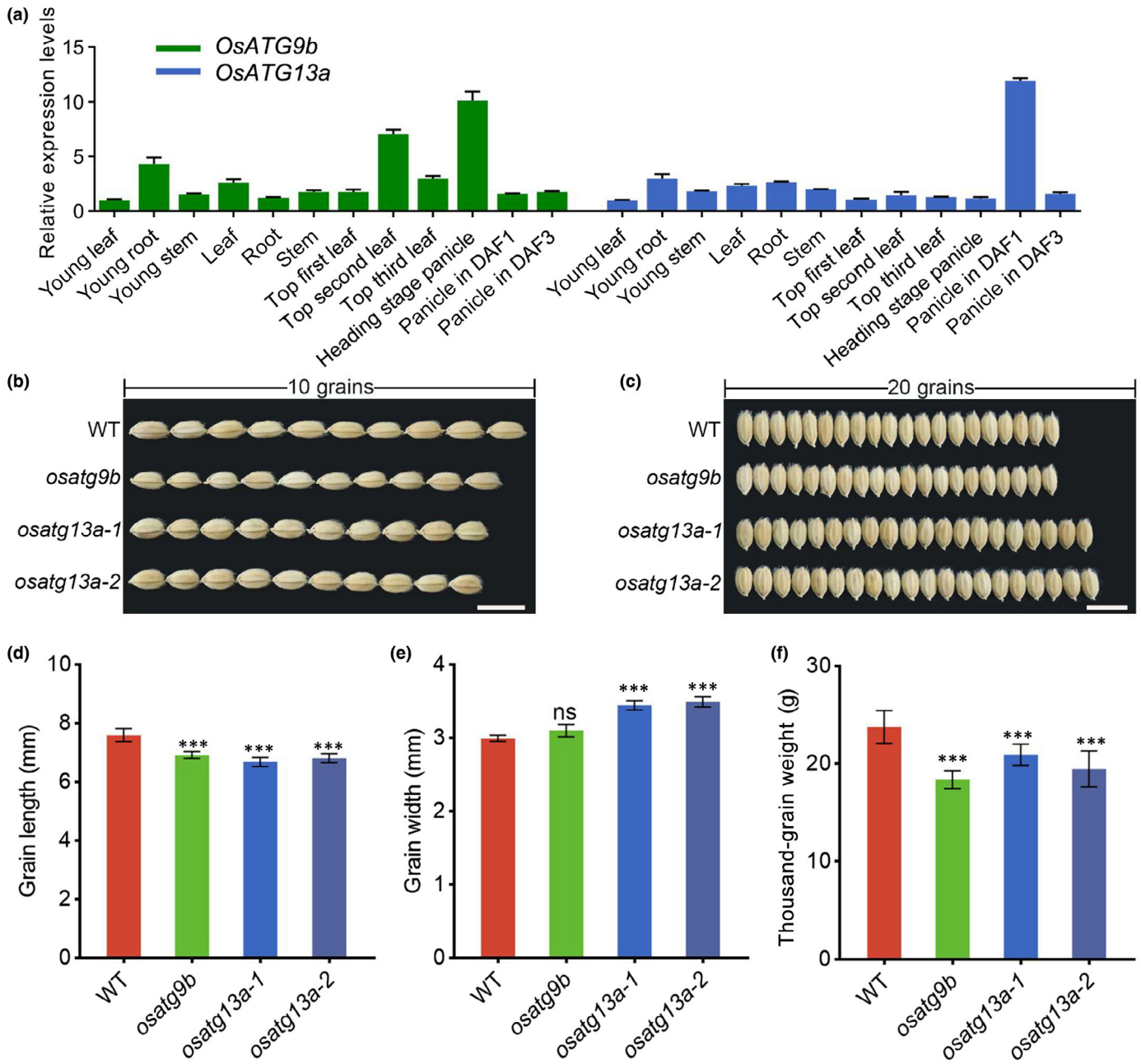

Fig. 1 Characterization of *osatg9b* and *osatg13a* grains. (a) Relative expression levels of *OsATG9b* and *OsATG13a* in various organs in rice (*Oryza sativa*). The relative expression level was normalized to *OsUBIQUITIN1* (*OsUBI1*, LOC_Os06g46770). The error bars represent SD ($n = 3$). (b, c) Representative images of grain length (b) and grain width (c) from wild-type (WT; ZH11), *osatg9b*, *osatg13a-1* and *osatg13a-2*. Bars, 1 cm. (d–f) Grain length (d), grain width (e) and thousand-grain weight (f) of the grains shown in (b, c; $n > 20$ plants, with at least 500 grains per plant). Data are means ± SD. Asterisks represent significant differences between mutants and WT by Student's *t*-test: ***, $P < 0.001$; ns, no significant difference.

5 cm stage (Fig. 2f), suggesting that the developmental cellular destiny (division and expansion) was perturbed in these mutants at an early developmental stage. Taken together, our results indicate that *OsATGs* modulate grain development at the early stage.

Contribution of OsATGs to both grain size and quality in rice

We also produced lines overexpressing *OsATG9b* (*OE-OsATG9b*) or *OsATG13a* (*OE-OsATG13a*) to confirm the role of these two genes in regulating grain development. Five independent overexpression lines of *OsATG9b* or *OsATG13a* were generated. The line 1 of *OsATG9b*-overexpressing plant (termed as *OE-OsATG9b*) with highest expressions of *OsATG9b* was selected for the following study (Fig. S2b), as well as the line 1 of *OsATG13a*-overexpressing plant (termed as *OE-OsATG13a*; Fig. S3b). Opposite from the *osatgs* mutants, both *OE-OsATG9b* and *OE-OsATG13a* lines produced bigger grains that were longer and wider to WT (Fig. 3a,c, d), and therefore heavier (Fig. 3e), indicating that the two genes indeed positively regulate grain size in rice. Previous study

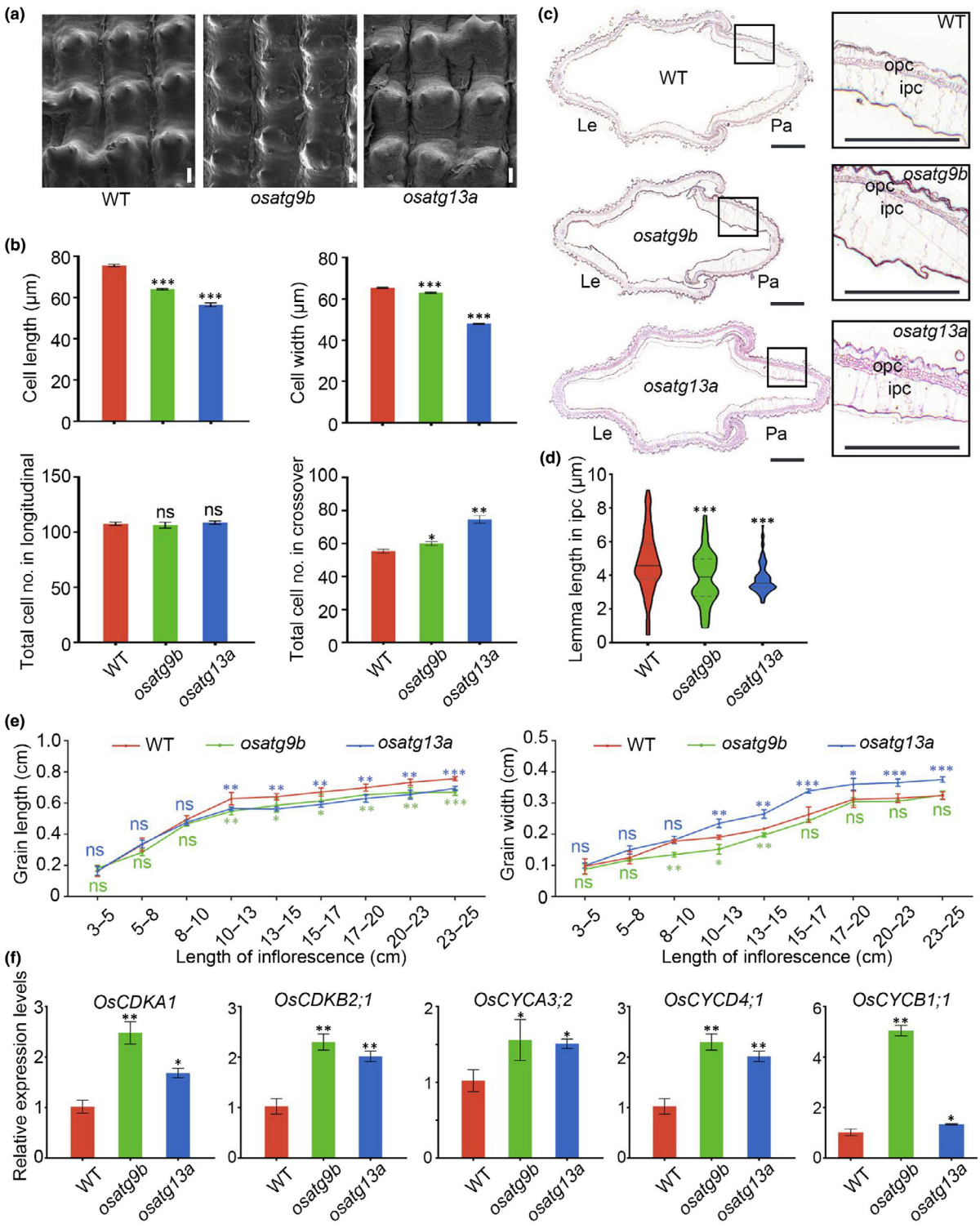

Fig. 2 Developmental analysis of *osatg9b* and *osatg13a* grains. (a) Scanning electron micrograph of the epidermal cell of wild-type (WT; *Oryza sativa* subsp. *japonica* cv Zhonghua 11), *osatg9b* and *osatg13a* spikelet hulls at the mature stage. Bars, 20 μm. (b) Cell length, cell width, cell number in longitudinal and cell number in crossover of grains shown in (a; $n \geq 3$ grains). (c) Cross-sections of inner parenchyma cells of WT, *osatg9b* and *osatg13a* spikelet hulls. Bars, 10 μm. ipc, inner parenchyma cells; Le, lemma; opc, out parenchymal cell; Pa, palea. (d) Ipc length in the palea of WT, *osatg9b* and *osatg13a* ($n \geq 75$). (e) Grain size of *osatg9b* and *osatg13a* at different developmental stages. Quantification of grain length (left) and grain width (right) in grain of WT, *osatg9b* and *osatg13a* from different length of florescence. The error bars represent SD ($n = 3$). (f) The relative expression levels of cell cycle genes in young panicles of WT, *osatg9b* and *osatg13a*. The relative expression level was normalized to *OsUBIQUITIN1* (*OsUBI1*, LOC_Os06g46770). The error bars represent SD ($n = 3$). *CDKA*, *Cyclin-Dependent Kinase A*; *CDKB2;1*, *Cyclin-Dependent Kinase B 2;1*; *CYCA3;2*, *Cyclin A 3;2*; *CYCB1;1*, *Cyclin B 1;1*; *CYCD4;1*, *Cyclin D 4;1*. Data are means ± SD. Asterisks represent significant differences between mutants and WT by Student's *t*-test: *, $P < 0.05$; **, $P < 0.01$; ***, $P < 0.001$; ns, no significant difference.

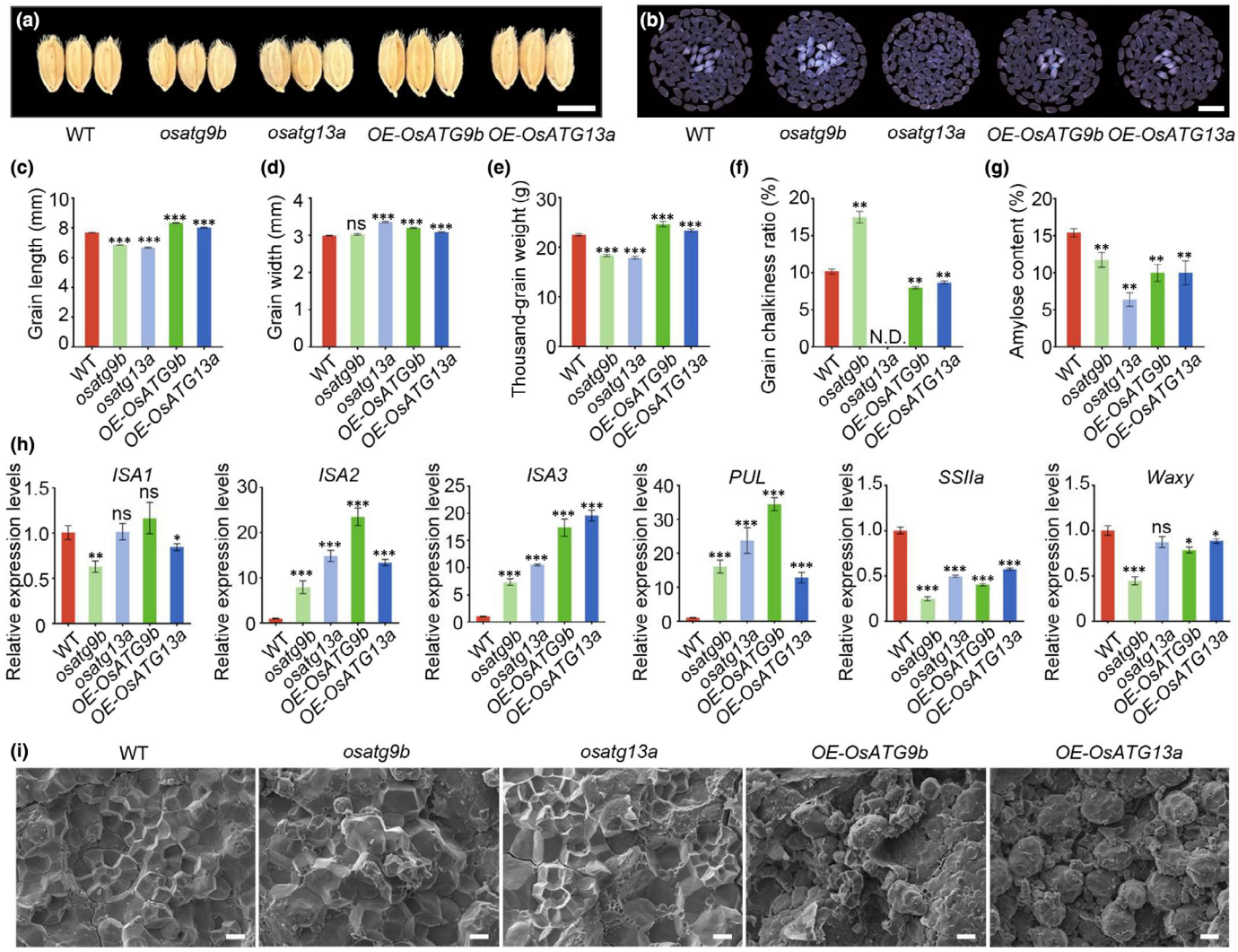

Fig. 3 Contribution of *OsATG9b* and *OsATG13a* to grain development. (a) Phenotypes of the grain length and grain width of wild-type (WT; *Oryza sativa* subsp. *japonica* cv Zhonghua 11), *osatg9b*, *osatg13a* (*osatg13a-1*, representative of *osatg13a*), *OE-OsATG9b* and *OE-OsATG13a*. Bar, 0.5 cm. (b) Milled rice morphology of WT, *osatg9b*, *osatg13a*, *OE-OsATG9b*, *OE-OsATG13a*. Bar, 2 cm. The rice was analyzed by the Rice Appearance Quality Detector. The white milled rice grains in the middle are the chalky grain. (c–e) Quantification of grain length (c), grain width (d) and thousand grain weight (e) of the grains in (a). The error bars represent SD ($n > 20$ plants). (f, g) Quantification of grain chalkiness (f) and amylose content (g) of WT, *osatg9b*, *osatg13a*, *OE-OsATG9b*, *OE-OsATG13a*. ND, not detected. (h) The relative expression levels of starch synthesis genes in 7 DAF panicles of WT, *osatg9b*, *osatg13a*, *OE-OsATG9b*, *OE-OsATG13a*. The relative expression level was normalized to *OsUBIQUITIN1* (*OsUBI1*, LOC_Os06g46770). The error bars represent SD ($n = 3$). DAF, day after fertilization; *ISA1*, *Isoamylase 1*; *ISA2*, *Isoamylase 2*; *ISA3*, *Isoamylase 3*; *PUL*, *Pullulanase*; *SSIIa*, *Starch synthase* (*SS*) *IIa*; *Wx*, *Waxy*. (i) Scanning electron micrographs of cracked mature caryopses of rice grains under different magnifications. Bars, 5 μm. Asterisks represent significant differences between transgenic lines and WT by Student's *t*-test: *, $P < 0.05$; **, $P < 0.01$; ***, $P < 0.001$; ns, no significant difference.

indicated that overexpressing *OsATG8b* increased the rice yield, which may be resulted from the altered grain size (Fan *et al.*, 2020). Here, we showed that the grain length was indeed increased in *OsATG8b*-overexpressing (*OE-OsATG8b*) rice (Fig. S11). Moreover, the dosage effect was shown in all of the *OsATG* overexpression lines (Figs S2, S3, S11).

Considering that change of grain size is generally accompanied by variation of grain quality (Kurusu *et al.*, 2014), we reasoned that autophagy might also modulate grain quality, which can be assessed by observing grain chalkiness. Chalkiness is caused by the accumulation of carbohydrate-derived starch granules (SGs) and is an undesirable appearance, quality, and milling quality trait in rice (Lisle *et al.*, 2000; Siebenmorgen *et al.*, 2013). The previous studies revealed that chalkiness was seen in *osatg7-1* and *OsATG8b*-RNAi (Sera *et al.*, 2019; Fan *et al.*, 2020). Here, our result showed that chalkiness was greater in *osatg9b* grains but less in *OE-OsATG9b* and *OE-OsATG13a* grains compared with WT grains (Fig. 3b,f). Higher chalkiness is associated with lower head rice yield (Fitzgerald *et al.*, 2009). Due to the irregular shape of most *osatg13a* grains, it was not possible to precisely evaluate chalkiness in this background (Figs 3b,f, S10). Amylose content (AC), which is determined by starch composition, is a crucial indicator of rice eating and cooking quality (Li *et al.*, 2016), which was significantly lower in *OE-OsATG9b* and *OE-*

OsATG13a grains compared with WT (Fig. 3g). We noticed a drop in AC in *osatg9b* and *osatg13a* (Fig. 3g). Amylose biosynthesis genes (*STARCH SYNTHASE IIa* (*SSIIa*) and *Waxy* (*WX*)) were expressed to lower levels in *OE-OsATGs* lines and *osatgs* mutants relative to WT, whereas amylopectin biosynthesis genes (*ISOAMYLASE 1* (*ISA1*), *ISA2*, *ISA3* and *PULLULANASE* (*PUL*)) were more highly expressed (Fig. 3h), eventually contributing to the lower AC seen in OE lines and *osatgs* mutants. The brown rice ratio and inferior head rice ratio were significantly higher in the *OE-OsATG9b* and *OE-OsATG13a* but lower in *osatg13a* compared with WT (Table S4), further suggesting that grain quality improved when *OsATGs* were overexpressed. SGs in cross-sections of *OE-OsATGs* lines were smaller and irregularly arranged compared to those in WT and *osatgs* mutants, which showed a polyhedral structure (Fig. 3i). Taken together, our results implicated that overexpression of *OsATGs* can potentially promote grain size, appearance quality, milling quality, and ECQ in rice.

Characterization of *OsATG9b* and *OsATG13a*

The functions of ATG9 and ATG13 in autophagy have been well-studied in Arabidopsis (*Arabidopsis thaliana*; Suttangkakul *et al.*, 2011; Zhuang *et al.*, 2017), but remain uncertain in rice. We wished to validate the roles of *OsATG9b* and *OsATG13a* in regulating autophagic activity. We transiently transfected protoplasts with the autophagic body marker RFP-OsATG8b, which underscored the differences in autophagic bodies in the various *osatgs* mutants and *OE-OsATGs*-lines. We detected fewer RFP-positive puncta in *osatg9b* or *osatg13a* protoplasts and more puncta in the ones of *OE-OsATG9b* and *OE-OsATG13a* following ConA treatment (Fig. 4a,b). Moreover, the number of GFP-OsATG8b-labeled autophagic bodies in *osatg9b* and *osatg13a* background was fewer than that of WT under concanamycin A (ConA; stabilize autophagic bodies in the vacuole and thus aids in their detection; Izumi *et al.*, 2015) or ConA plus wortmannin (wort; it can inhibit autophagy; Izumi *et al.*, 2015) treatments (Fig. 4c,d). Furthermore, the autofluorescent drug MDC staining, a specific indicator labeling acid vesicles, primarily autophagosomes (Contento *et al.*, 2005), detected significantly fewer autophagosomes in both *osatgs* mutants but more autophagosome vesicles in *OE-OsATG9b* and *OE-OsATG13a* background as compared to WT after treatment (Fig. S12). All the results indicated that *OsATG9b* and *OsATG13a* participate in the autophagy process.

Free GFP assay is typically used to measure autophagic influx, because the GFP fusion protein is often rapidly released proteolytically and degraded once inside the vacuole, whereas the freed GFP is substantially more stable and accumulates; therefore, the ratio of free GFP to fused GFP provides a quantitative measure of autophagic flux, and the appearance or absence of GFP easily confirm that a potential autophagic substrate is degraded by autophagy (Huang *et al.*, 2019). Accordingly, we determined the ratio of free GFP to GFP-OsATG8b in various *osatgs* mutants backgrounds at seedling stage and seed developing stage. We detected lower abundance for both GFP-OsATG8b and free GFP in *osatg9b* and *osatg13a* mutant seedlings grown under normal conditions, although their free GFP : GFP-OsATG8b ratio was comparable to that of WT (Fig. 4e,f). After an 8-d period of growth in darkness to induce autophagy, the abundance of free GFP and GFP-OsATG8b, as well as the ratio of free GFP : GFP-OsATG8b, significantly decreased in both *osatgs* mutants relative to WT (Fig. 4e,f). Furthermore, the significant reduction of the ratio of free GFP : GFP-OsATG8b in both *osatg9b* and *osatg13a* compared with WT was shown during the DAF1 to DAF5 (Fig. S13), indicating that *OsATG9b* and *OsATG13a* are required for autophagic influx during seed developing stages.

Detection of ATG8-PE (phosphatidylethanolamine) is another stringent criterion that reflects the autophagic flux (Marshall & Vierstra, 2018). Using the ATG8-antibody, our immunoblotting analyses revealed that OsATG8-PE abundance was higher in *osatg9b* and *osatg13a*, but lower in *osatg5* or *osatg7* (Fig. 4g,h), in agreement with a previous study (Chung *et al.*, 2010; Zhuang *et al.*, 2017), indicating that *OsATG9b* and *OsATG13a* are functional in autophagic machinery.

Furthermore, we tested the subcellular localization of *OsATG9b* and *OsATG13a*. *OsATG9b-GFP* is colocalized with the Golgi marker, mCherry-AtRER1B (Fig. S14a; Sato *et al.*, 1999; Takeuchi *et al.*, 2000), which is consistent with previous studies (Suttangkakul *et al.*, 2011; Zhuang *et al.*, 2017). The localization of ATG13 was not reported before; hence, we assessed the subcellular localization of *OsATG13a* by cotransfecting rice protoplasts with constructs encoding the fusion protein *OsATG13a-GFP* and AtTZF1-mCherry (Cytoplasmic Foci, CF marker; M. C. Pomeranz *et al.*, 2010), OsRac3 (Plasma Membrane, PM marker; Chen *et al.*, 2010), KTI1 (ER marker; Jofuku & Goldberg, 1989) or mCherry-AtRER1B (Sato *et al.*, 1999; Takeuchi *et al.*, 2000). Our results revealed that *OsATG13a-GFP* is highly colocalized with the CF marker, which was reported to be localized in processing bodies (M. C. Pomeranz *et al.*, 2010), rather than other markers (Fig. S14b). In agreement with the notion that ATG9 and ATG13a contribute to the initiation and formation of autophagosomes in the cytoplasm (Suttangkakul *et al.*, 2011; Zhuang *et al.*, 2017), we determined that *OsATG9b-GFP* and *OsATG13a-GFP* also colocalized with the autophagosome marker RFP (red fluorescent protein)-OsATG8b (Fig. S14c; Fan *et al.*, 2020). We therefore propose that *OsATG9b* and *OsATG13a* are likely to be responsible for the biogenesis of autophagosomes in the cytoplasm in rice. Together, we concluded that the *OsATG9b* and *OsATG13a* positively regulate autophagy, and thus the changes in grain size and quality of the *osatgs* and *OE-OsATGs* were predominately resulted from the corresponding variations of autophagy activity.

Identification of TGW6 as the OsATG8-interacting protein

Given autophagy is implicated to be charge of protein turnover, we then speculated that autophagy modulates grain growth by selectively degrading certain grain associated regulators. To address this issue, we performed a Y2H assay to identify proteins interacting with the core autophagy component OsATG8b, which yielded TGW6 as a candidate (Table S5). ATG8-

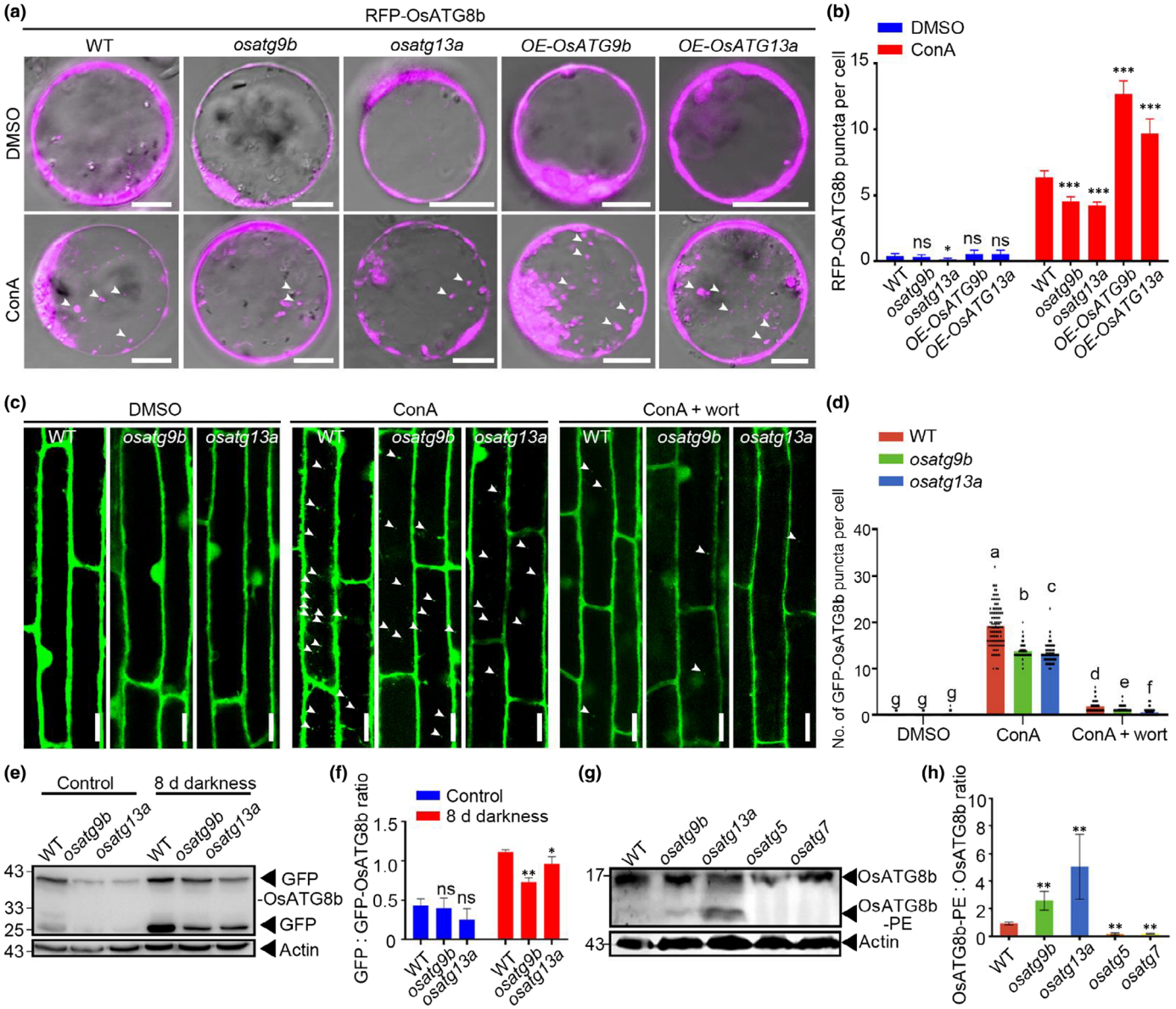

Fig. 4 *OsATG9b* And *OsATG13a* positively regulate autophagy. (a, b) Transient expression of RFP-OsATG8b fusion protein in rice protoplasts of wild-type (WT; *Oryza sativa* subsp. *japonica* cv Zhonghua 11), *osatg9b*, *osatg13a*, *OE-OsATG9b*, *OE-OsATG13a*. The rice protoplasts were treated with ConA or DMSO for 12-h darkness and observed by confocal microscopy (a). The white arrows indicate part of RFP-OsATG8b-labeled autophagic bodies that appeared as red puncta in vacuole. Bars, 10 μm. Quantification of puncta in the protoplasts (b) were observed using epifluorescence microscopy, with at least 25 protoplasts observed per transgenic plant for each condition (a). (c, d) Detection of punctate GFP-OsATG8b-labeled autophagic bodies (up) in WT, *osatg9b*, *osatg13a*. Five-day-old seedlings were treated with DMSO, wortmannin, and/or ConA for 12-h darkness (c). After treatment the puncta per root cell was calculated by ImageJ (d). The white arrows indicate part of autophagic bodies appearing as green puncta within cells. ConA, Concanamycin A. Bars, 10 μm. The number of puncta (down) in each image was counted and averaged from at least 100 cells of per transgenic plant for each condition. (e, f) Anti-GFP immunoblot (e) was performed using protein extracts of WT or *osatgs* seedlings expressing pUBI::GFP-OsATG8b. Eight-day-old seedlings were incubated under normal condition or dark condition for 8 d before protein extraction. Anti-Actin immunoblots are shown as loading control. Quantification of the protein bands (f) shown in (e). The GFP : GFP-OsATG8b ratio was determined by the intensity of free GFP moiety bands, normalized by the corresponding intensity of full-length GFP-OsATG8b bands ($n = 3$ biological replicates). (g, h) Detection of OsATG8b-PE of WT and *osatgs* seedlings. The seedlings of WT, *osatg9b*, *osatg13a*, *osatg5* and *osatg7* were incubated under darkness for 8 d and examined for the production of OsATG8b-PE by urea-SDS-PAGE and immunoblotting using anti-ATG8 antibodies (g). Quantification of the protein bands (h) shown in (g). The OsATG8b-PE : OsATG8b ratio was determined by the intensity of OsATG8b-PE moiety bands, normalized by the corresponding intensity of full-length OsATG8b bands ($n = 3$ biological replicates). The error bars represent SD. Asterisks represent significant differences between transgenic lines and WT by Student's *t*-test: *, $P < 0.05$; **, $P < 0.01$; ***, $P < 0.001$; ns, no significant difference.

interacting proteins generally possess canonical AIMs (Liu *et al.*, 2021). We detected seven putative AIMs in TGW6 by iLIR analysis (https://ilir.warwick.ac.uk/index.php; Kalvari *et al.*, 2014; Jacomin *et al.*, 2016; Table S6), further implying that it might be the substrate candidate in terms of selective autophagy-mediated grain development. To test this possibility,

we first examined that interaction between TGW6 and OsATG8s (represented by the four OsATG8 isoforms OsATG8a, OsATG8b, OsATG8c, and OsATG8d) by targeted Y2H, showing that they interacted with each other (Fig. S15a). Next, pull-down assay was conducted to validate TGW6-OsATG8s interaction, indicating that they interacted with each other *in vitro* (Fig. S15b). In addition, the BiFC was also performed to confirm the interaction between TGW6 and OsATG8s (Fig. S15c). Moreover, the LUC assay further proved that TGW6 indeed interacted with OsATG8s *in vivo* (Fig. S15d). As mentioned above that TGW6 possesses putative AIMs, we then verified whether TGW6 interacts with OsATG8s dependent on AIM-LDS (LIR/AIM docking site) but not UIM-UDS (UIM docking site) manner. As a result, mutation of the LDS (Y50A L51A in OsATG8a (△LDS)) rather than UDS (I77A V78A V79A in OsATG8a (△UDS)) in OsATG8a (as a representative) absolutely blocked its interaction with TGW6 (Fig. S15e), indicating that TGW6 interacts with OsATG8 via the canonical AIM-LDS manner. Furthermore, the AIM2 (DAYMGL) with anchor potential and AIM3 (GYWIAL) with highest PSSM score in TGW6 by the iLIR analysis (Jacomin *et al.*, 2016; Table S6) were selected for further investigation of their associations with OsATG8. To test the role of AIM2 and AIM3 in OsATG8 binding, we mutated the key residues of AIM2 (TGW6$^{\triangle AIM2}$:Y148A L150A) or AIM3 (TGW6$^{\triangle AIM3}$:W282A L284A) to alanine within full-length TGW6 (Fig. 5a), and performed Y2H, BiFC, pull-down, and LUC assays between OsATG8b and these TGW6 variants. TGW6$^{\triangle AIM2}$ no longer interacted with OsATG8b, whereas TGW6$^{\triangle AIM3}$ still interacted with OsATG8b (Fig. 5b–e). These results demonstrate that AIM2 of TGW6 is essential for the OsATG8-TGW6 interaction.

Considering that autophagy generally employs ATG8 to transport a target protein to the autophagosome for degradation (Marshall & Vierstra, 2018), we hypothesized that TGW6 might be recruited by OsATG8s to the autophagosome for selective degradation. To test the above hypothesis, we transiently expressed a construct encoding mCherry-TGW6 in *N. benthamiana* leaves and then treated them with ConA. We detected many mCherry-TGW6 puncta within vacuoles upon ConA treatment compared with the DMSO control (Fig. S15f,g). We also observed the colocalization of mCherry-TGW6 puncta with the autophagic body marker EGFP (enhanced green fluorescent protein)-OsATG8b in the vacuole (Fan *et al.*, 2020) after ConA treatment (Fig. S15h). Together, our results demonstrate that TGW6 is recruited by OsATG8s and then delivered to autophagic machinery for selective degradation in vacuole. We next examined whether AIM2 is required for the degradation of TGW6 by detecting mCherry-TGW6$^{\triangle AIM2}$ and TGW6$^{\triangle AIM3}$ puncta within vacuoles upon ConA treatment compared with the DMSO control. As shown in Fig. 5(f), we observed that TGW6$^{\triangle AIM3}$ rather than TGW6$^{\triangle AIM2}$ puncta were colocalized with OsATG8b-labled autophagic bodies within vacuole upon ConA treatment, indicating that AIM2 mutation of TGW6 disturbs its delivery into autophagosomes. Therefore, we concluded that AIM2, but not AIM3, is necessary for the autophagic degradation of TGW6.

Control of TGW6-mediated grain development by selective autophagy

We speculated that autophagy may control TGW6 homeostasis to regulate grain development. To further confirm above idea, we evaluated TGW6 abundance in *osatgs* mutants and *OE-OsATGs* lines by producing a specific polyclonal anti-TGW6 antibody (Fig. S4b). Using this antibody, we observed that TGW6 protein gradually accumulated in WT grains from 1 to 5 d after fertilization (DAF), in accordance with a previous study (Fig. 6a,b; Ishimaru *et al.*, 2013). By contrast, TGW6 was more abundant in *osatg9b* and *osatg13a* grains but accumulated to lower levels in *OE-OsATG9b* and *OE-OsATG13a* grains compared with WT (Fig. 6a, b). In addition, similar decrease of TGW6 was also detected in *OE-OsATG8b* lines in comparable of that in WT during grain development (Fig. S16), further indicating that TGW6 homeostasis is controlled by autophagy during grain development.

To investigated whether TGW6 was the sole regulator of grain size being degraded by autophagy, we then isolated the double-knockout mutants *tgw6 osatg9b*, *tgw6 osatg13a-1*, *tgw6 osatg13a-2*, and *tgw6 osatg13a-3* by knocking out *TGW6* in the *osatg9b* and *osatg13a-1* background (Fig. S1c). Immunoblotting analyses revealed that TGW6 protein was totally eliminated in *tgw6*, *tgw6 osatg9b*, *tgw6 osatg13a-1*, *tgw6 osatg13a-2*, and *tgw6 osatg13a-3* mutants (Fig. S17). The shorter grain length seen in *osatg9b* or *osatg13a* was only partially rescued in *tgw6 osatg9b* and *tgw6 osatg13a*, and was significantly shorter than that of the *tgw6* single mutant (Fig. 6c,d). With respect to grain width, we observed no significant difference between the double knockout mutants and their respective *osatg9b* or *osatg13a-1* mutants (Fig. 6c,e). Taken all together, our results elaborate that selective autophagy modulates the grain size and quality at least by degrading TGW6, and other grain size regulators might also be degraded via autophagy during grain development (Fig. 7).

Discussion

There is a long-lasting paradox between grain size and quality since increasing grain size for high yield is generally accompanied by increase of carbohydrates derived high starch and chalkiness in endosperm (Li *et al.*, 2019), ultimately leading to the decrease in taste quality. In this study, we demonstrate that autophagy contributes to both grain size and quality by selective degradation of TGW6, thereby dissecting a potential exploitation of autophagy in rice breeding.

Autophagy is operated by multiple ATGs and related components, which are highly conserved among various species (Marshall & Vierstra, 2018). Our results indicate that either *OsATG9b* or *OsATG13a* positively regulate grain length and width by activating the autophagy activity, suggesting that manipulation of *ATG* genes or autophagy related components may have similar effects in various crop, especially cereal crop. This possibility would greatly expand gene resources for sustainably improving grain size and quality.

The ATG1/13 kinase complex is the key regulator of autophagy induction, which initiates autophagosome formation in

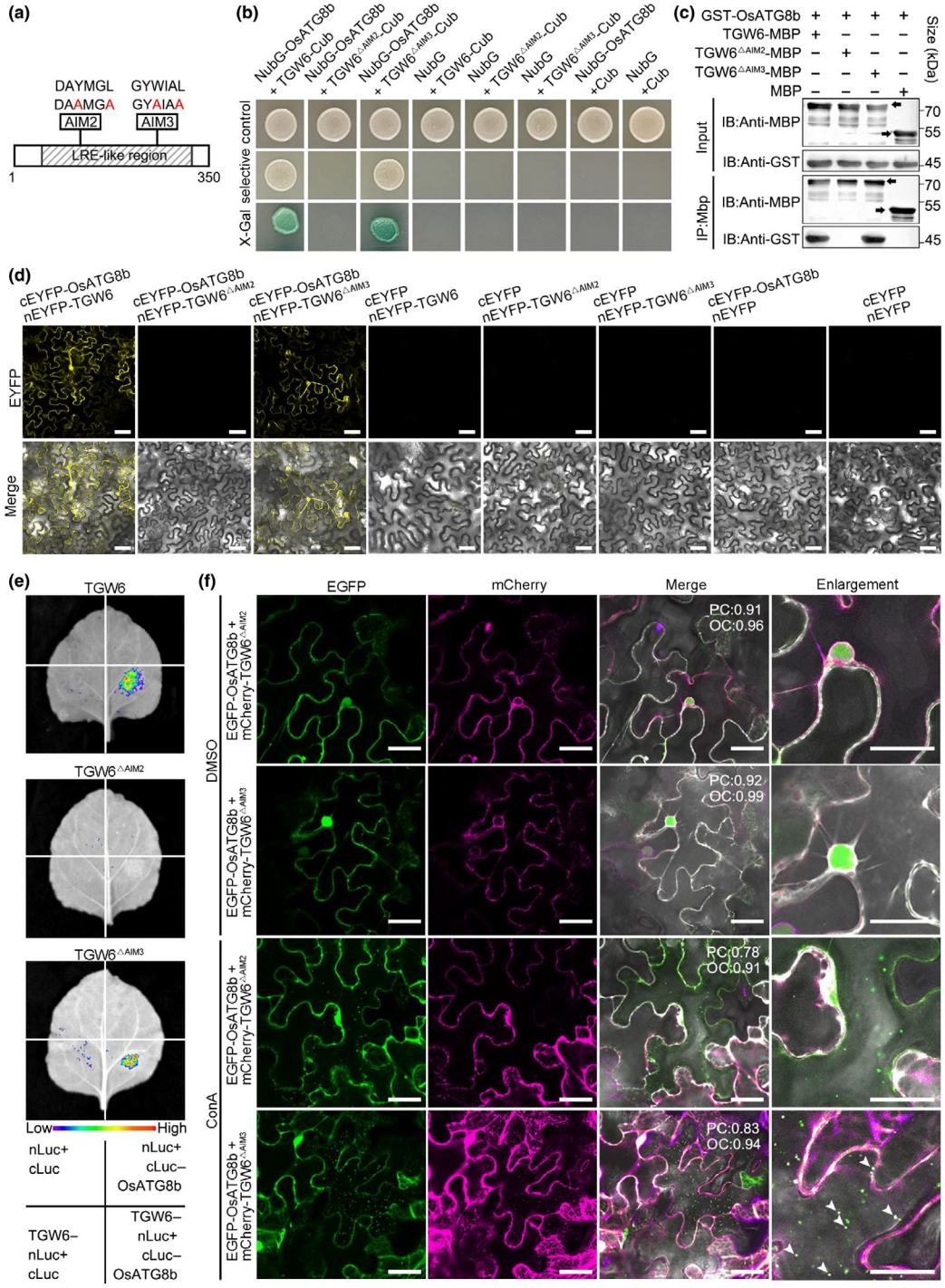

Fig. 5 The AIM2 sequence is required for the TGW6-OsATG8 interaction and the autophagic degradation of TGW6. (a) Schematic representation of putative ATG8-interacting motifs (AIMs: W/L/Y–X–X–L/I/V) in TGW6, including AIM2 and AIM3 predicted by iLIR (up), as well as the mutated AIM2 and AIM3 (down). Red text represents the substituted amino acid of the AIMs in TGW6. (b) Yeast-two hybrid (Y2H) assays between TGW6$^{\triangle AIM2}$ or TGW6$^{\triangle AIM3}$ and OsATG8b. The transformants were plated on control medium (SD/−Trp–Leu medium) or seletetive medium (SD/−Trp–Leu–His–Ade medium) with or without X-Gal. (c) The interactions of TGW6, TGW6$^{\triangle AIM2}$ or TGW6$^{\triangle AIM3}$ with OsATG8b were detected by immunoblot with anti-GST after MBP pull-down. TGW6-MBP, TGW6$^{\triangle AIM2}$-MBP and TGW6$^{\triangle AIM3}$-MBP was detected using anti-MBP antibody. GST-OsATG8b was detected using anti-GST antibody. (d) Bimolecular fluorescence complementation (BiFC) assays of TGW6, TGW6$^{\triangle AIM2}$ or TGW6$^{\triangle AIM3}$ with OsATG8b in *Nicotiana benthamiana*. Bars, 20 μm. (e) Luciferase complementation (LUC) assays of TGW6, TGW6$^{\triangle AIM2}$ or TGW6$^{\triangle AIM3}$ with OsATG8b. nLUC-tagged TGW6, nLUC-tagged TGW6$^{\triangle AIM2}$ or nLUC-tagged TGW6$^{\triangle AIM3}$ with cLUC-tagged OsATG8b were co-transformed into tobacco (*N. benthamiana*) leaves. (f) Representative images showing colocalization of EGFP-OsATG8b with mCherry-TGW6$^{\triangle AIM2}$ or mCherry-TGW6$^{\triangle AIM3}$ in tobacco (*N. benthamiana*) leaf cell. Leaves were treated with DMSO or 1 μM ConA under 12-h darkness conditions and imaged by confocal microscopy (OC, overlap coefficient; PC, Pearson's correlation). ConA, Concanamycin A. The puncta in the vacuole were the EGFP-OsATG8b-labled autophagic bodies. The white arrows indicate puncta where GFP and mCherry signals overlap in vacuole. Bars, 10 μm. These experiments were repeated three times with similar results.

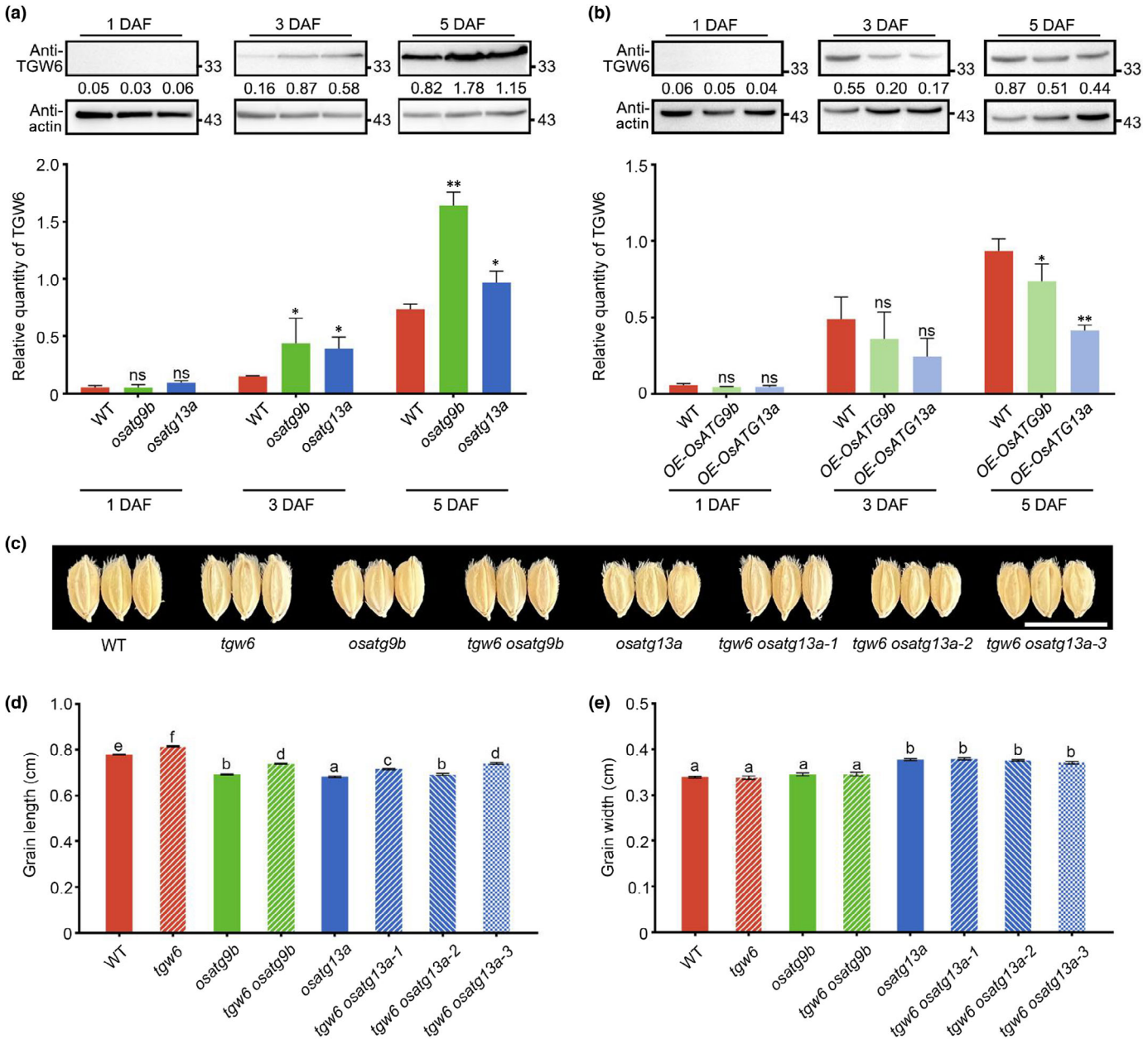

Fig. 6 Relative quantity of TGW6 and genetic analysis. (a, b) The pattern of relative quantity of TGW6 (up) in panicle of WT (*Oryza sativa* subsp. *japonica* cv Zhonghua 11), *osatg9b*, *osatg13a*, *OE-OsATG9b*, *OE-OsATG13a* from 1, 3, 5 d after fertilization (DAF). TGW6 protein abundance was determined by immunoblotting. Actin was used as loading control. Relative quantity of TGW6 (down) was based on the density analysis of immunoblots using ImageJ. The error bars represent SD ($n = 3$ biological replicates). Asterisks represent significant differences by Student *t*-test: *, $P < 0.05$; **, $P < 0.01$; ns, no significant difference. (c–e) Phenotypes (c) of the knockout mutant *osatg9b*, *osatg13a* and double knockout mutant *tgw6 osatg9b*, *tgw6 osatg13a-1*, *tgw6 osatg13a-2*, *tgw6 osatg13a-3*. Bar, 1 cm. Quantification of grain length (d) and grain width (e) of the grains in (c). The error bars represent SD ($n = 50$ grains). Different letters indicate the significant differences determined by one-way ANOVA ($P < 0.05$).

response to nutrient demands. However, it is still unclear where this complex senses the stress signals to activate autophagy. Therefore, we were particularly interested in verifying the subcellular localization of *OsATG13a*. By assessing the colocalization of *OsATG13a* with different organelles markers, we propose that *OsATG13a* likely localizes in the cytoplasmic foci (CF; Fig. S14b). In eukaryotic cells, when mRNAs fail to pass the quality control or translation is repressed, mRNAs cannot be translated or degraded in the cytoplasm after being exported from the nucleus, and thus mRNA-protein complexes are temporarily stored in CFs, also known as processing bodies (PBs; M. Pomeranz *et al.*, 2010). Upon nutrient starvation, CFs/PBs were formed and autophagy was activated, leading to the growth arrest and translation repression of the cell (Marshall & Vierstra, 2018; Guzikowski *et al.*, 2019). Notably, the CF components DExD/H-box RNA helicase (Dhh1) directly associates with ATG1 and ATG13 mRNAs and facilitates their translations under nitrogen starvation conditions, thereby ensuring the proper level of

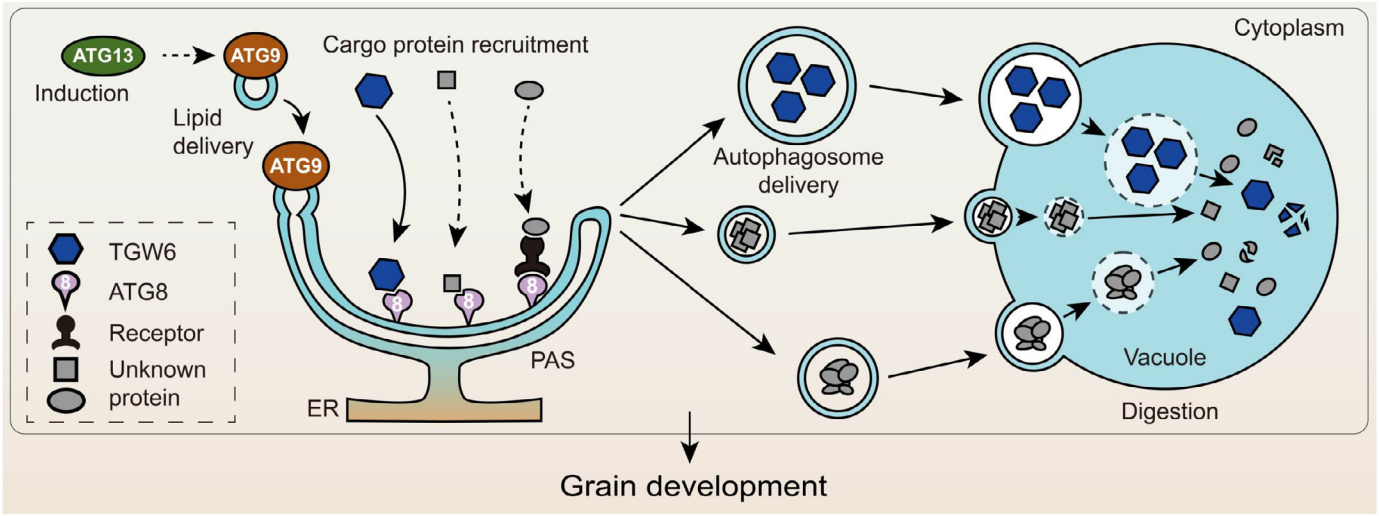

Fig. 7 Proposed model of the selective autophagy of TGW6 in the regulation grain size in rice (*Oryza sativa*). ATG13 is responsible for the initiation of autophagy during grain development. Once the autophagy activated, ATG9 mediates the delivery of lipid to the emerging phagophore, leading to the expansion of membranes and vesicle nucleation. Meanwhile, ATG8 interacts with cargo receptors or proteins, such as TGW6 and other unknown grain size proteins, and then transports them into the autophagosomes for degradation within the vacuole, finally determining the grain size and quality in rice. Dashed arrows, regulations identified in this study; dotted arrows, putative regulations. ER, endoplasmic reticulum; PAS, phagophore assembly site.

autophagy in the face of nitrogen starvation (Hurto & Hopper, 2011; Liu *et al.*, 2019). Therefore, we postulate that *OsATG13a* may be synthesized in CFs upon sensing the nutrient starvation signals and then activates the autophagy.

In this study, we identified the TGW6 as one of the autophagy substrates in terms of the grain development. Similar to many known autophagy substrates that possess AIM (Hu *et al.*, 2022; Shao *et al.*, 2022), we also demonstrate that the AIM2 in TGW6 is critical for the TGW6-OsATG8 interaction. Mutation of the AIM2 impaired the TGW6-OsATG8 interaction (Fig. 5b–e), and also blocked TGW6 degradation (Fig. 5f), indicating that the AIM2 is essential for autophagy-mediated TGW6 degradation.

Previous study elaborated that TGW6 encodes an Investment Adviser Association (IAA)-glucose hydrolase, which can hydrolyze IAA-glucose into IAA and glucose by liquid chromatography-electrospray ionization-tandem mass spectrometry (Ishimaru *et al.*, 2013). Surprisingly, a recent research suggested that OsTGW6 and TaTGW6 might not regulate grain size via the hydrolysis of IAA-glucose, because OsTGW6 and its clade I homologues are expressed in early inflorescences but not in developing kernels by microarray data analysis and RNA-seq analyses, as well as wheat grains had undetectable levels of ester IAA in comparison with free IAA (Kabir & Nonhebel, 2021). However, we found that increased levels of TGW6 were detected in panicles of DAF1, DAF3, and DAF5 by Western blotting analyses (Figs 6a, S16), suggesting that TGW6 functions in developing seeds.

Indeed, our results demonstrated that autophagy is operated in the developing seeds (Fig. S13). As a result, the loss of *OsATG9b* and *OsATG13a* function in the *osatgs* mutant results in impaired autophagy and thus blocks the autophagic degradation of TGW6 in the developing seeds, leading to increased TGW6 levels in the developing seeds in the *osatgs* mutant (Fig. 6a). By contrast, the TGW6 levels was reduced in the developing seeds of *OE-OsATGs* lines that possess higher autophagy level (Figs 6b, S16). Together, we propose that autophagy monitors TGW6 homeostasis for determining the final grain size.

It has been implicated that less starch content but chalky appearance was identified in *osatg7-1* and *osatg8b* grain endosperm (Sera *et al.*, 2019; Fan *et al.*, 2020), while overexpression of *OsATG8b* showed no variation of starch (Fan *et al.*, 2020). Interestingly, less chalkiness was found in the *OE-OsATGs* grains in this study (Fig. 3b,f), presumably the higher expression of *OsATGs* the less chalkiness. Notably, SGs in cross-sections of *OE-OsATGs* lines (Fig. 3i) were reminiscent of the *tgw6* mutant (Han *et al.*, 2018), suggesting that *OsATGs* modulate grain quality by degrading TGW6. In addition, *OE-OsATGs* also produces the bigger grain (Fig. 3a,c,d). Therefore, dramatically boosting *OsATGs* may be an efficient strategy to simultaneously promote grain appearance and taste quality.

Notably, genetic analysis demonstrated that TGW6 is not the sole target for autophagy underlying grain size regulation, because the grain defect of *osatgs* mutants is unable to be fully restored by knockout of *TGW6* (Fig. 6c,d), suggesting there may be other substrates controlled by autophagy during grain development. Similar to the TGW6, several key negative regulators of grain size, including the TGW3 (Ying *et al.*, 2018), Grain Size 3 (GS3; Fan *et al.*, 2006), and Grain Length 3.1 (GL3.1)/qGL3 (Qi *et al.*, 2012; Zhang *et al.*, 2012), seem containing the putative AIMs if identified by iLIR analysis, implying they may be also recruited by OsATG8 for autophagic degradation during the grain development in rice.

In summary, our results demonstrate that the abundance of TGW6, and perhaps that of other grain size regulators are fine-tuned by OsATGs-mediated selective autophagy during grain

development (Fig. 7). Therefore, manipulation of the ATGs-TGW6 axis (and perhaps other grain size factors) may be applicable for further improving grain size and quality in crops.

Acknowledgements

We are grateful to Dr Linchuan Liu (South China Agricultural University) for kind help on immunoblotting analysis, and Drs Chun Wang and Kejian Wang (China National Rice Research Institute) for assisting on the generation of *osatg9b* and *osatg13a* mutant, as well as the valuable comments from Dr Faqiang Li (South China Agricultural University) and Dr Chengcai Chu (South China Agricultural University). This work was supported by the open competition program of top 10 critical priorities of Agricultural Science and Technology Innovation for the 14th Five-Year Plan of Guangdong Province (grant 2022SDZG05 to QX), the National Natural Science Foundation of China (31971920 to QX and YH), the Major Program of Guangdong Basic and Applied Research (2019B030302006 to QX), and the Guangdong Basic and Applied Basic Research Foundation (2021A1515012053 to QX), as well as the supports from the State Key Laboratory for Conservation and Utilization of Subtropical Agro-bioresources (SKLCUSA-a202008 to QX and Y Liu), the Special Plan for Key Laboratory of 'Western Light Western cross team' (xbzg-zdsys-202111 to PX and QX), the 'Top Young Scientist of the Pearl River Talent Plan' (no. 20170104 to QX) and the Double first-class discipline promotion project (2021B10564001 to QY).

Competing interests

A patent has been approved (no. ZL202010418636.3) based on the results reported in this paper.

Author contributions

QX conceived and designed the experiments. ZL performed most experiments. QY, PW, Y Li and Y Lin characterized the *osatgs* mutants and *OE-OsATGs* lines with assistance of WL, SG, Y Liu, YH and PX. YQ produced most of the transgenic plants. QX, QY and ZL analyzed the data, wrote and revised the manuscript. All authors read and commented on the paper. ZL, QY, PW, Y Li and Y Lin contributed equally to this work.

ORCID

Yunfeng Liu https://orcid.org/0000-0002-4166-9056
Yangwen Qian https://orcid.org/0000-0002-7062-3495
Qingjun Xie https://orcid.org/0000-0002-6372-3260
Peng Xu https://orcid.org/0000-0003-1064-6721
Qianying Yang https://orcid.org/0000-0003-1628-571X

Data availability

The authors declare that all data supporting the findings of this study are available within the paper and its Supporting Information.

References

Butardo VM, Sreenivasulu N, Juliano BO. 2019. Improving rice grain quality: state-of-the-art and future prospects. *Rice Grain Quality: Methods and Protocols* **1892**: 19–55.

Chen L, Shiotani K, Togashi T, Miki D, Aoyama M, Wong HL, Kawasaki T, Shimamoto K. 2010. Analysis of the Rac/Rop small GTPase family in rice: expression, subcellular localization and role in disease resistance. *Plant and Cell Physiology* **51**: 585–595.

Chumpen Ramirez S, Gómez-Sánchez R, Verlhac P, Hardenberg R, Margheritis E, Cosentino K, Reggiori F, Ungermann C. 2023. Atg9 interactions via its transmembrane domains are required for phagophore expansion during autophagy. *Autophagy* **19**: 1–20.

Chung T, Phillips AR, Vierstra RD. 2010. ATG8 lipidation and ATG8-mediated autophagy in *Arabidopsis* require ATG12 expressed from the differentially controlled ATG12A and ATG12B loci. *The Plant Journal* **62**: 483–493.

Contento AL, Xiong Y, Bassham DC. 2005. Visualization of autophagy in *Arabidopsis* using the fluorescent dye monodansylcadaverine and a GFP-AtATG8e fusion protein. *The Plant Journal* **42**: 598–608.

Erlichman OA, Weiss S, Abu Arkia M, Ankary-Khaner M, Soroka Y, Jasinska W, Rosental L, Brotman Y, Avin-Wittenberg T. 2023. Autophagy in maternal tissues contributes to *Arabidopsis* seed development. *Plant Physiology* **193**: kiad350.

Fan C, Xing Y, Mao H, Lu T, Han B, Xu C, Li X, Zhang Q. 2006. GS3, a major QTL for grain length and weight and minor QTL for grain width and thickness in rice, encodes a putative transmembrane protein. *Theoretical and Applied Genetics* **112**: 1164–1171.

Fan T, Yang W, Zeng X, Xu X, Xu Y, Fan X, Luo M, Tian C, Xia K, Zhang M. 2020. A rice autophagy gene *OsATG8b* is involved in nitrogen remobilization and control of grain quality. *Frontiers in Plant Science* **11**: 588.

Farré J-C, Kramer M, Ideker T, Subramani S. 2017. Active interaction mapping as a tool to elucidate hierarchical functions of biological processes. *Autophagy* **13**: 1248–1249.

Fitzgerald MA, McCouch SR, Hall RD. 2009. Not just a grain of rice: the quest for quality. *Trends in Plant Science* **14**: 133–139.

Fujioka Y, Alam JM, Noshiro D, Mouri K, Ando T, Okada Y, May AI, Knorr RL, Suzuki K, Ohsumi Y. 2020. Phase separation organizes the site of autophagosome formation. *Nature* **578**: 301–305.

Guo J, Wang H, Guan W, Guo Q, Wang J, Yang J, Peng Y, Shan J, Gao M, Shi S. 2023. A tripartite rheostat controls self-regulated host plant resistance to insects. *Nature* **618**: 1–9.

Guzikowski AR, Chen YS, Zid BM. 2019. Stress-induced mRNP granules: form and function of processing bodies and stress granules. *Wiley Interdisciplinary Reviews: RNA* **10**: e1524.

Han J, Ma K, Li H, Su J, Zhou L, Tang J, Zhang S, Hou Y, Chen L, Liu YG. 2022. All-in-one: a robust fluorescent fusion protein vector toolbox for protein localization and BiFC analyses in plants. *Plant Biotechnology Journal* **20**: 1098–1109.

Han Y, Luo D, Usman B, Nawaz G, Zhao N, Liu F, Li R. 2018. Development of high yielding glutinous cytoplasmic male sterile rice (*Oryza sativa* L.) lines through CRISPR/Cas9 based mutagenesis of *Wx* and *TGW6* and proteomic analysis of anther. *Agronomy* **8**: 290.

He Y, Sun S, Zhao J, Huang Z, Peng L, Huang C, Tang Z, Huang Q, Wang Z. 2023. UDP-glucosyltransferase OsUGT75A promotes submergence tolerance during rice seed germination. *Nature Communications* **14**: 2296.

Hu Z, Yang Z, Zhang Y, Zhang A, Lu Q, Fang Y, Lu C. 2022. Autophagy targets Hd1 for vacuolar degradation to regulate rice flowering. *Molecular Plant* **15**: 1137–1156.

Huang X, Zheng C, Liu F, Yang C, Zheng P, Lu X, Tian J, Chung T, Otegui MS, Xiao S. 2019. Genetic analyses of the *Arabidopsis* ATG1 kinase complex reveal both kinase-dependent and independent autophagic routes during fixed-carbon starvation. *Plant Cell* **31**: 2973–2995.

Hurto RL, Hopper AK. 2011. P-body components, Dhh1 and Pat1, are involved in tRNA nuclear-cytoplasmic dynamics. *RNA* **17**: 912–924.

Ishimaru K, Hirotsu N, Madoka Y, Murakami N, Hara N, Onodera H, Kashiwagi T, Ujiie K, Shimizu B-i, Onishi A. 2013. Loss of function of the

IAA-glucose hydrolase gene TGW6 enhances rice grain weight and increases yield. *Nature Genetics* **45**: 707–711.

Izumi M, Hidema J, Wada S, Kondo E, Kurusu T, Kuchitsu K, Makino A, Ishida H. 2015. Establishment of monitoring methods for autophagy in rice reveals autophagic recycling of chloroplasts and root plastids during energy limitation. *Plant Physiology* **167**: 1307–1320.

Jacomin A-C, Samavedam S, Promponas V, Nezis IP. 2016. iLIR database: a web resource for LIR motif-containing proteins in eukaryotes. *Autophagy* **12**: 1945–1953.

Jofuku KD, Goldberg RB. 1989. Kunitz trypsin inhibitor genes are differentially expressed during the soybean life cycle and in transformed tobacco plants. *Plant Cell* **1**: 1079–1093.

Kabir MR, Nonhebel HM. 2021. Reinvestigation of *THOUSAND-GRAIN WEIGHT 6* grain weight genes in wheat and rice indicates a role in pollen development rather than regulation of auxin content in grains. *Theoretical and Applied Genetics* **134**: 2051–2062.

Kalvari I, Tsompanis S, Mulakkal NC, Osgood R, Johansen T, Nezis IP, Promponas VJ. 2014. iLIR: a web resource for prediction of Atg8-family interacting proteins. *Autophagy* **10**: 913–925.

Kurusu T, Koyano T, Hanamata S, Kubo T, Noguchi Y, Yagi C, Nagata N, Yamamoto T, Ohnishi T, Okazaki Y. 2014. *OsATG7* is required for autophagy-dependent lipid metabolism in rice postmeiotic anther development. *Autophagy* **10**: 878–888.

Li F, Chung T, Pennington JG, Federico ML, Kaeppler HF, Kaeppler SM, Otegui MS, Vierstra RD. 2015. Autophagic recycling plays a central role in maize nitrogen remobilization. *Plant Cell* **27**: 1389–1408.

Li F, Chung T, Vierstra RD. 2014. AUTOPHAGY-RELATED11 plays a critical role in general autophagy-and senescence-induced mitophagy in *Arabidopsis*. *Plant Cell* **26**: 788–807.

Li H, Prakash S, Nicholson TM, Fitzgerald MA, Gilbert RG. 2016. The importance of amylose and amylopectin fine structure for textural properties of cooked rice grains. *Food Chemistry* **196**: 702–711.

Li N, Xu R, Li Y. 2019. Molecular networks of seed size control in plants. *Annual Review of Plant Biology* **70**: 435–463.

Lisle A, Martin M, Fitzgerald M. 2000. Chalky and translucent rice grains differ in starch composition and structure and cooking properties. *Cereal Chemistry* **77**: 627–632.

Liu W, Liu Z, Mo Z, Guo S, Liu Y, Xie Q. 2021. ATG8-interacting motif: evolution and function in selective autophagy of targeting biological processes. *Frontiers in Plant Science* **12**: 783881.

Liu X, Yao Z, Jin M, Namkoong S, Yin Z, Lee JH, Klionsky DJ. 2019. Dhh1 promotes autophagy-related protein translation during nitrogen starvation. *PLoS Biology* **17**: e3000219.

Livak KJ, Schmittgen TD. 2001. Analysis of relative gene expression data using real-time quantitative PCR and the $2^{-\Delta\Delta CT}$ method. *Methods* **25**: 402–408.

Luo N, Shang D, Tang Z, Mai J, Huang X, Tao LZ, Liu L, Gao C, Qian Y, Xie Q *et al.* 2023. Engineered ATG8-binding motif-based selective autophagy to degrade proteins and organelles in planta. *New Phytologist* **237**: 684–697.

Mao T, Zhu M, Sheng Z, Shao G, Jiao G, Mawia AM, Ahmad S, Xie L, Tang S, Wei X. 2021. Effects of grain shape genes editing on appearance quality of erect-panicle geng/japonica rice. *Rice* **14**: 1–7.

Marshall RS, Hua Z, Mali S, McLoughlin F, Vierstra RD. 2019. ATG8-binding UIM proteins define a new class of autophagy adaptors and receptors. *Cell* **177**: 766–781.

Marshall RS, Vierstra RD. 2018. Autophagy: the master of bulk and selective recycling. *Annual Review of Plant Biology* **69**: 173–208.

Matoba K, Kotani T, Tsutsumi A, Tsuji T, Mori T, Noshiro D, Sugita Y, Nomura N, Iwata S, Ohsumi Y. 2020. Atg9 is a lipid scramblase that mediates autophagosomal membrane expansion. *Nature Structural & Molecular Biology* **27**: 1185–1193.

Nguyen A, Faesen AC. 2023. The role of the HORMA domain proteins ATG13 and ATG101 in initiating autophagosome biogenesis. *FEBS Letters* **597**. doi: 10.1002/1873-3468.14717.

Noda NN, Ohsumi Y, Inagaki F. 2010. Atg8-family interacting motif crucial for selective autophagy. *FEBS Letters* **584**: 1379–1385.

Nolan TM, Brennan B, Yang M, Chen J, Zhang M, Li Z, Wang X, Bassham DC, Walley J, Yin Y. 2017. Selective autophagy of BES1 mediated by DSK2 balances plant growth and survival. *Developmental Cell* **41**: 33–46.

Olivas TJ, Wu Y, Yu S, Luan L, Choi P, Guinn ED, Nag S, De Camilli PV, Gupta K, Melia TJ. 2023. ATG9 vesicles comprise the seed membrane of mammalian autophagosomes. *Journal of Cell Biology* **222**: e202208088.

Park S-G, Park H-S, Baek M-K, Jeong J-M, Cho Y-C, Lee G-M, Lee C-M, Suh J-P, Kim C-S, Kim S-M. 2019. Improving the glossiness of cooked rice, an important component of visual rice grain quality. *Rice* **12**: 1–13.

Pomeranz M, Lin P-C, Finer J, Jang J-C. 2010. AtTZF gene family localizes to cytoplasmic foci. *Plant Signaling & Behavior* **5**: 190–192.

Pomeranz MC, Hah C, Lin P-C, Kang SG, Finer JJ, Blackshear PJ, Jang J-C. 2010. The *Arabidopsis* tandem zinc finger protein AtTZF1 traffics between the nucleus and cytoplasmic foci and binds both DNA and RNA. *Plant Physiology* **152**: 151–165.

Pu Y, Bassham DC. 2016. Detection of autophagy in plants by fluorescence microscopy. *Plant Proteostasis: Methods and Protocols* **2581**: 161–172.

Qi H, Lei X, Wang Y, Yu S, Liu T, Zhou S-K, Chen J-Y, Chen Q-F, Qiu R-L, Jiang L. 2022. 14-3-3 proteins contribute to autophagy by modulating SINAT-mediated degradation of ATG13. *Plant Cell* **34**: 4857–4876.

Qi P, Lin Y-S, Song X-J, Shen J-B, Huang W, Shan J-X, Zhu M-Z, Jiang L, Gao J-P, Lin H-X. 2012. The novel quantitative trait locus *GL3. 1* controls rice grain size and yield by regulating Cyclin-T1; 3. *Cell Research* **22**: 1666–1680.

Ren D, Ding C, Qian Q. 2023. Molecular bases of rice grain size and quality for optimized productivity. *Science Bulletin* **68**: 314–350.

Sato K, Ueda T, Nakano A. 1999. The *Arabidopsis thaliana* RER1 gene family: its potential role in the endoplasmic reticulum localization of membrane proteins. *Plant Molecular Biology* **41**: 815–824.

Sera Y, Hanamata S, Sakamoto S, Ono S, Kaneko K, Mitsui Y, Koyano T, Fujita N, Sasou A, Masumura T. 2019. Essential roles of autophagy in metabolic regulation in endosperm development during rice seed maturation. *Scientific Reports* **9**: 18544.

Shao W-Q, Zhu W-W, Luo M-J, Fan M-H, Li Q, Wang S-H, Lin Z-F, Zhao J, Zheng Y, Dong Q-Z. 2022. Cholesterol suppresses GOLM1-dependent selective autophagy of RTKs in hepatocellular carcinoma. *Cell Reports* **39**: 110712.

Siebenmorgen TJ, Grigg BC, Lanning SB. 2013. Impacts of preharvest factors during kernel development on rice quality and functionality. *Annual Review of Food Science and Technology* **4**: 101–115.

Song T, Shi Y, Shen L, Cao C, Shen Y, Jing W, Tian Q, Lin F, Li W, Zhang W. 2021. An endoplasmic reticulum–localized cytochrome b_5 regulates high-affinity K^+ transport in response to salt stress in rice. *Proceedings of the National Academy of Sciences, USA* **118**: e2114347118.

Sparkes IA, Runions J, Kearns A, Hawes C. 2006. Rapid, transient expression of fluorescent fusion proteins in tobacco plants and generation of stably transformed plants. *Nature Protocols* **1**: 2019–2025.

Suttangkakul A, Li F, Chung T, Vierstra RD. 2011. The ATG1/ATG13 protein kinase complex is both a regulator and a target of autophagic recycling in *Arabidopsis*. *Plant Cell* **23**: 3761–3779.

Takeuchi M, Ueda T, Sato K, Abe H, Nagata T, Nakano A. 2000. A dominant negative mutant of sar1 GTPase inhibits protein transport from the endoplasmic reticulum to the Golgi apparatus in tobacco and *Arabidopsis* cultured cells. *The Plant Journal* **23**: 517–525.

Wada S, Hayashida Y, Izumi M, Kurusu T, Hanamata S, Kanno K, Kojima S, Yamaya T, Kuchitsu K, Makino A. 2015. Autophagy supports biomass production and nitrogen use efficiency at the vegetative stage in rice. *Plant Physiology* **168**: 60–73.

Wu B, Yun P, Zhou H, Xia D, Gu Y, Li P, Yao J, Zhou Z, Chen J, Liu R. 2022. Natural variation in *WHITE-CORE RATE 1* regulates redox homeostasis in rice endosperm to affect grain quality. *Plant Cell* **34**: 1912–1932.

Xia K, Liu T, Ouyang J, Wang R, Fan T, Zhang M. 2011. Genome-wide identification, classification, and expression analysis of autophagy-associated gene homologues in rice (*Oryza sativa* L.). *DNA Research* **18**: 363–377.

Yang C, Shen S, Zhou S, Li Y, Mao Y, Zhou J, Shi Y, An L, Zhou Q, Peng W. 2022. Rice metabolic regulatory network spanning the entire life cycle. *Molecular Plant* **15**: 258–275.

Yao W, Li Y, Chen Y, Chen Y, Zhao P, Zhang Y, Jiang Q, Feng Y, Yang F, Wu C. 2023. Mec1 regulates PAS recruitment of Atg13 via direct binding with

Atg13 during glucose starvation-induced autophagy. *Proceedings of the National Academy of Sciences, USA* **120**: e2215126120.

Ying J-Z, Ma M, Bai C, Huang X-H, Liu J-L, Fan Y-Y, Song X-J. 2018. TGW3, a major QTL that negatively modulates grain length and weight in rice. *Molecular Plant* **11**: 750–753.

Yu J, Zhen X, Li X, Li N, Xu F. 2019. Increased autophagy of rice can increase yield and nitrogen use efficiency (NUE). *Frontiers in Plant Science* **10**: 584.

Zeng D, Ma X, Xie X, Zhu Q, Liu Y. 2018. A protocol for CRISPR/Cas9-based multi-gene editing and sequence decoding of mutant sites in plants. *Scientia Sinica Vitae* **48**: 783–794.

Zhang X, Wang J, Huang J, Lan H, Wang C, Yin C, Wu Y, Tang H, Qian Q, Li J. 2012. Rare allele of OsPPKL1 associated with grain length causes extra-large grain and a significant yield increase in rice. *Proceedings of the National Academy of Sciences, USA* **109**: 21534–21539.

Zhang Y, Su J, Duan S, Ao Y, Dai J, Liu J, Wang P, Li Y, Liu B, Feng D. 2011. A highly efficient rice green tissue protoplast system for transient gene expression and studying light/chloroplast-related processes. *Plant Methods* 7: 1–14.

Zhuang X, Chung KP, Cui Y, Lin W, Gao C, Kang B-H, Jiang L. 2017. ATG9 regulates autophagosome progression from the endoplasmic reticulum in *Arabidopsis*. *Proceedings of the National Academy of Sciences, USA* **114**: E426–E435.

Supporting Information

Additional Supporting Information may be found online in the Supporting Information section at the end of the article.

Fig. S1 Schematic representative of various *osatg* single mutants, *tgw6 osatg9b* and *tgw6 osatg13a* double mutants generated by the CRISPR/Cas9.

Fig. S2 Characterization of *OE-OsATG9b* grains in different lines.

Fig. S3 Characterization of *OE-OsATG13a* grains in different lines.

Fig. S4 Determination of the specificity of OsATG8-antibody and TGW6-antibody.

Fig. S5 Heatmap representation of the expression of the 24 predicted *OsATGs* across various tissues in rice.

Fig. S6 Agronomic traits of *osatg9b* and *osatg9b-C*.

Fig. S7 Genetic complementation of *osatg9b*.

Fig. S8 Agronomic traits of *osatg13a*.

Fig. S9 Functional redundancy analyses in *osatg9b* and *osatg13a*.

Fig. S10 Seed morphology of various *osatgs* and *OsATGs*-overexpressing lines during grain filling stages.

Fig. S11 Characterization of *OE-OsATG8b* grains in different lines.

Fig. S12 Monodansylcadaverine staining of rice root in various *osatgs* and *OsATGs*-overexpressing lines with DMSO or ConA treatments.

Fig. S13 Autophagic flux analysis of *osatgs'* panicle by the GFP-ATG8 processing assay.

Fig. S14 Colocalization analyses of *OsATG9b* and *OsATG13a*.

Fig. S15 Identification of TGW6 as an autophagy substrate.

Fig. S16 Relative quantity of TGW6 in *OE-OsATG8b* lines.

Fig. S17 Detection of TGW6 in the DAF5 panicle of double-knockout mutants.

Table S1 Target sequences of the CRISPR/Cas9 editing of the corresponding mutants.

Table S2 Primers used for vector construction.

Table S3 Primers used for RT-qPCR analysis.

Table S4 Effects of shading on starch pasting viscosity of rice flour.

Table S5 List of candidate proteins identified by yeast two-hybrid screen.

Table S6 Putative Atg8-interacting motifs in TGW6.

Please note: Wiley is not responsible for the content or functionality of any Supporting Information supplied by the authors. Any queries (other than missing material) should be directed to the *New Phytologist* Central Office.